Separation and Purification Technology 354 (2025) 129358

Contents lists available at ScienceDirect

Separation and Purification Technology

journal homepage: www.elsevier.com/locate/seppur

Stepwise customizing pore environments of C_2H_2-selective frameworks for one-step C_2H_4 acquisition from ternary mixtures

Shuixiang Zou [a,b], Cheng Chen [a], Zhengyi Di [a], Yuanzheng Liu [a], Hengbo Li [a], Yashuang Li [a], Rajamani Krishna [c], Daqiang Yuan [a], Mingyan Wu [a,b,*]

[a] State Key Lab of Structural Chemistry, Fujian Institute of Research on the Structure of Matter, Chinese Academy of Sciences, Fuzhou, Fujian 350002, China
[b] University of Chinese Academy of Sciences, Beijing, 100049, China
[c] Van't Hoff Institute for Molecular Sciences, University of Amsterdam, Science Park 904, 1098 XH Amsterdam, the Netherlands

ARTICLE INFO

Keywords:
Metal-organic framework
Gas separation
One-step C_2H_4 purification
C_2H_2-selective material

ABSTRACT

One-step purification of C_2H_4 from ternary $C_2H_2/C_2H_4/C_2H_6$ mixture is crucial but challenging since the primary physical properties of C_2H_4 all fall between C_2H_2 and C_2H_6. Hence, we report an effective approach for purifying C_2H_4 through stepwise customizing pore environments on C_2H_2-selective materials. Utilizing **SIFSIX-1-Cu** as a prototype material, we incorporated one or two methoxyl groups onto 4,4′-bipyridine to obtain isomorphic framework **SIFSIX-1-Cu-OMe** and **SIFSIX-1-Cu-(OMe)$_2$** respectively. As expected, pore sizes gradually decrease, while C_2H_6 binding sites increase. Ultimately, the C_2H_6/C_2H_4 (10/90) selectivity gradually increases from 1.18 (**SIFSIX-1-Cu**) to 1.27 (**SIFSIX-1-Cu-OMe**) and finally to a remarkably high value of 1.79 (**SIFSIX-1-Cu-(OMe)$_2$**). As anticipated, **SIFSIX-1-Cu-(OMe)$_2$** can achieve one-step acquisition of polymer-grade C_2H_4 (≥99.95 %) from $C_2H_2/C_2H_4/C_2H_6$ (1/90/9) mixture with high productivity of 6.82 L/kg. Furthermore, theoretical calculations indicate that the pore surface of **SIFSIX-1-Cu-(OMe)$_2$** is beneficial to preferentially capture C_2H_2 and C_2H_6, and thus realizes one-step purification of C_2H_4.

1. Introduction

As the most important chemical raw material, ethylene (C_2H_4) is widely used in the preparation of basic chemicals such as polyethylene, vinyl chloride and styrene [1–4]. Naphtha or ethane thermal cracking is the main method to produce C_2H_4, but impurities such as acetylene (C_2H_2) and ethane (C_2H_6) are inevitably present in the product [5,6]. The current industry standard for separation involves the utilization of low temperature and high pressure technology to remove C_2H_6, followed by catalytic hydrogenation or solvent extraction to eliminate C_2H_2, which is not only energy-consuming but also environmentally unfriendly [7–9]. Therefore, it is imperative to develop an efficient and energy-saving separation method to realize the one-step purification of C_2H_4 from ternary mixture of $C_2H_2/C_2H_4/C_2H_6$.

Metal-organic frameworks (MOFs) have become the star materials for purifying C_2H_4 due to their tunable frameworks and customizable pore structures. In recent years, MOFs have made significant progress in binary gas mixuture separation such as C_2H_2/C_2H_4 [10–14] and C_2H_4/C_2H_6 separation [15–18]. Regarding the ternary $C_2H_2/C_2H_4/C_2H_6$ mixture, the molecule size and quadrupole moment of C_2H_4 (4.2 Å and 1.5×10^{-26} esu·cm^2) are intermediate between those of C_2H_2 (3.3 Å and 7.2×10^{-26} esu·cm^2) and C_2H_6 (4.4 Å and 0.65×10^{-26} esu·cm^2), which not only eliminates the possibility of molecular sieving, but also presents a challenge to the one-step purification of C_2H_4 through thermodynamic separation [19,20]. At present, only several examples, which have stronger binding sites for C_2H_2 and C_2H_6 simultaneously compared with C_2H_4, can realize one-step C_2H_4 acquisition from ternary $C_2H_2/C_2H_4/C_2H_6$ mixture [21–26]. However, rationally designing an adsorbent with high selectivity for both C_2H_2/C_2H_4 and C_2H_6/C_2H_4 are extremely difficult. In contrast, pore engineering strategies based on C_2H_2-selective or C_2H_6-selective MOFs, such as ligand functionalization, offers greater potential for achieving one-step C_2H_4 acquisition from a mixture of C_2-hydrocarbons. Some successful instances, which introduce the C_2H_2 binding sites into C_2H_6-selective MOFs to enhance C_2H_2/C_2H_4 selectivity, have been reported [27,28]. Noteworthy, MOFs which show inverse adsorption of C_2H_6 and C_2H_4 are uncommon. Therefore, engineering the pore of a C_2H_6-selective material for one-step acquisition of C_2H_4 from $C_2H_2/C_2H_4/C_2H_6$ mixture is of great difficulty and not

* Corresponding author.
E-mail address: wumy@fjirsm.ac.cn (M. Wu).

https://doi.org/10.1016/j.seppur.2024.129358
Received 29 June 2024; Received in revised form 13 August 2024; Accepted 23 August 2024
Available online 25 August 2024
1383-5866/© 2024 Elsevier B.V. All rights are reserved, including those for text and data mining, AI training, and similar technologies.

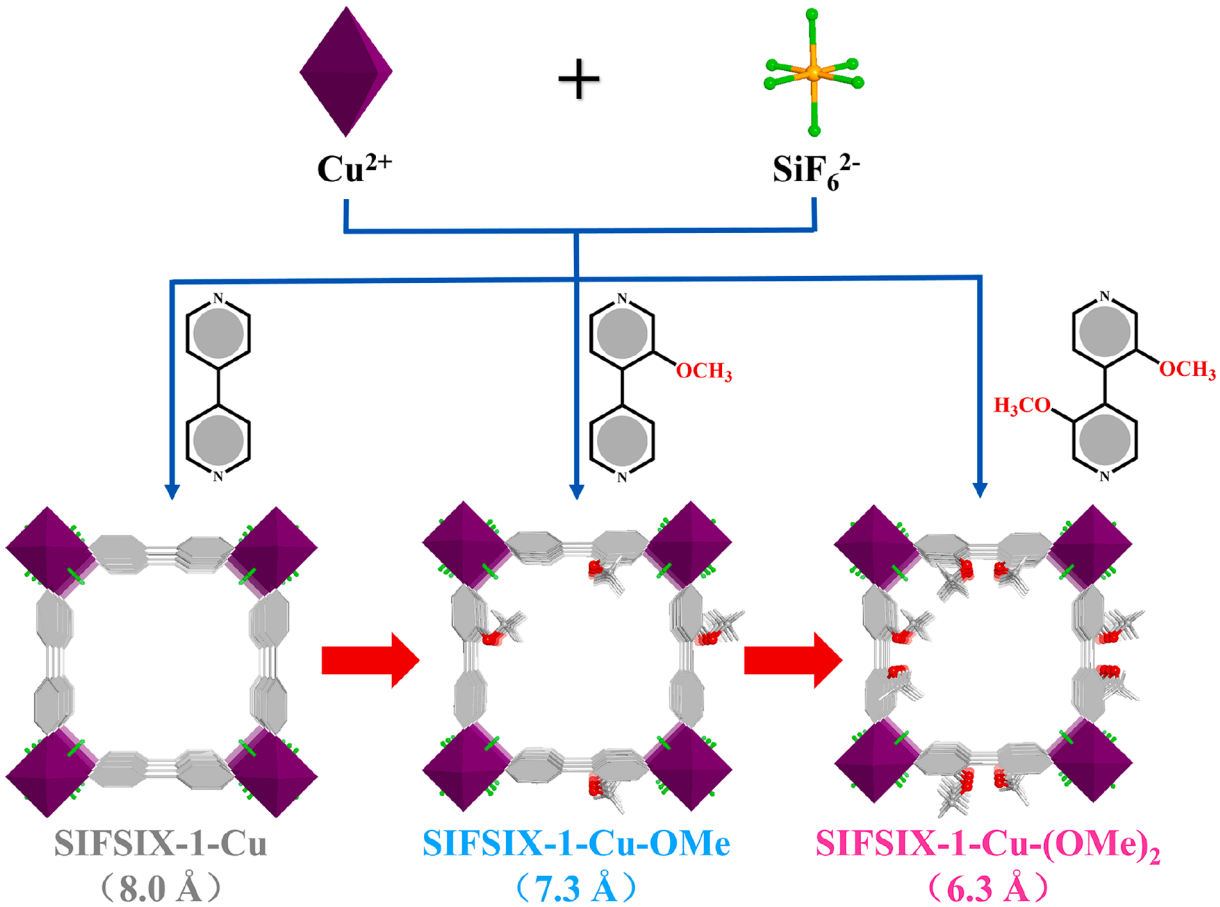

Fig. 1. Structural description of **SIFSIX-1-Cu**, **SIFSIX-1-Cu-OMe** and **SIFSIX-1-Cu-(OMe)$_2$**. Colour code: Cu (purple), Si (orange), F (green), C (grey), N (blue), O (red) and H (white).

feasible. In view of the fact that C_2H_2 has more π-electrons and smaller molecule size, it is observed that most reported MOFs exhibit a stronger affinity towards C_2H_2 compared with C_2H_4, which can realize the efficeint separation of C_2H_2/C_2H_4. Considering the easy availability, C_2H_2-selective MOFs may be used as the prototype materials for pore engineering. However, such examples are rarely reported, because it is extremely difficult to achieve preferential adsorption of C_2H_6 over C_2H_4 while maintain high C_2H_2/C_2H_4 selectivity [29].

The anion-pillared fluorinated hybrid materials, which demonstrate specific recognition of C_2H_2 due to the strong interactions between the C_2H_2 and electronegative F atoms, exhibit benchmark separation capability for C_2H_2/C_2H_4 [30–34]. More importantly, the pore dimension and environment can be fine-tuned by pore engineering strategies [35–40]. Therefore, they are a kind of promising adsorbents whose pore structures can be tailored to preferentially capture C_2H_2 and C_2H_6. For example, the typical SIFSIX material, **SIFSIX-1-Cu**, not only can be easily synthesized from inexpensive feedstocks with a stable framework, but also shows exceptional C_2H_2 adsorption capacity as well as high C_2H_2/C_2H_4 selectivity. As we know, C_2H_6 has higher polarizability and more hydrogen atoms compared with C_2H_4 (44.7×10^{-25} vs 42.52×10^{-25} cm^3). Therefore, by enlarging the non-polar/inert pore surfaces or introducing multiple O/N binding sites on the suitable pore walls, more supramolecular interactions (C-H…π interactions or C-H…O/N interactions) can be formed between C_2H_6 and the framework, which enables preferential adsorption of C_2H_6 over C_2H_4 [41–45].

In this work, we report an example of stepwise customizing pore environments on the C_2H_2-selective materials to enable one-step purification of C_2H_4 from ternary mixture of $C_2H_2/C_2H_4/C_2H_6$. Stepwise introduction of one and two methoxyl (–OCH_3) groups into **SIFSIX-1-Cu**, results in decreasing pore size from 8.0 Å (**SIFSIX-1-Cu**) to 7.3 Å (**SIFSIX-1-Cu-OMe**) and then to 6.3 Å (**SIFSIX-1-Cu-(OMe)$_2$**). At 298 K and 0.1 bar, **SIFSIX-1-Cu** shows almost equal adsorption amount of C_2H_6 and C_2H_4, and the adsorption difference as well as the C_2H_6/C_2H_4 uptake ratio are only 1.7 cm^3/g and 117 % respectively. With the progressive augmentation of the number of modified –OCH_3 groups, these values gradually enhance to 3.1 cm^3/g and 130 % (**SIFSIX-1-Cu-OMe**), and reach the maximum in **SIFSIX-1-Cu-(OMe)$_2$** (8.2 cm^3/g and 171 %) at 298 K and 0.1 bar. Furthermore, the difference of isosteric adsorption heats (ΔQ_{st}) for C_2H_4 and C_2H_6 decreases from 5.0 kJ/mol (**SIFSIX-1-Cu**) to 0.2 kJ/mol (**SIFSIX-1-Cu-OMe**). As anticipated, **SIFSIX-1-Cu-(OMe)$_2$** exhibits reverse-order adsorption of C_2H_6 and C_2H_4, accompanied with the ΔQ_{st} difference value of -2.2 kJ/mol. More importantly, the C_2H_6/C_2H_4 (10/90) IAST selectivity is significantly improve from 1.18 (**SIFSIX-1-Cu**) to 1.27 (**SIFSIX-1-Cu-OMe**), and finally reaches a remarkably high value of 1.79 (**SIFSIX-1-Cu-(OMe)$_2$**). Dynamic breakthrough experiments demonstrate that **SIFSIX-1-Cu** and **SIFSIX-1-Cu-OMe** cannot realize the one-step C_2H_4 purification from ternary $C_2H_2/C_2H_4/C_2H_6$ (1/90/9) mixture due to the simultaneous outflow of C_2H_4 and C_2H_6. In contrast, under the same condition, **SIFSIX-1-Cu-(OMe)$_2$** exhibits obviously C_2H_6/C_2H_4 separation with breakthrough time interval up to 14 min/g, and enables one-step access to polymer-grade C_2H_4 (≥99.95 %) from 1/90/9 $C_2H_2/C_2H_4/C_2H_6$ with a high productivity of 6.82 L/kg. Computational simulations reveal that the optimal pore surface of **SIFSIX-1-Cu-(OMe)$_2$** with suitable pore size and multiple O binding sites exhibits preferential affinity for capturing C_2H_2 and C_2H_6, thereby enabling the one-step purification of C_2H_4 from $C_2H_2/C_2H_4/C_2H_6$ mixture.

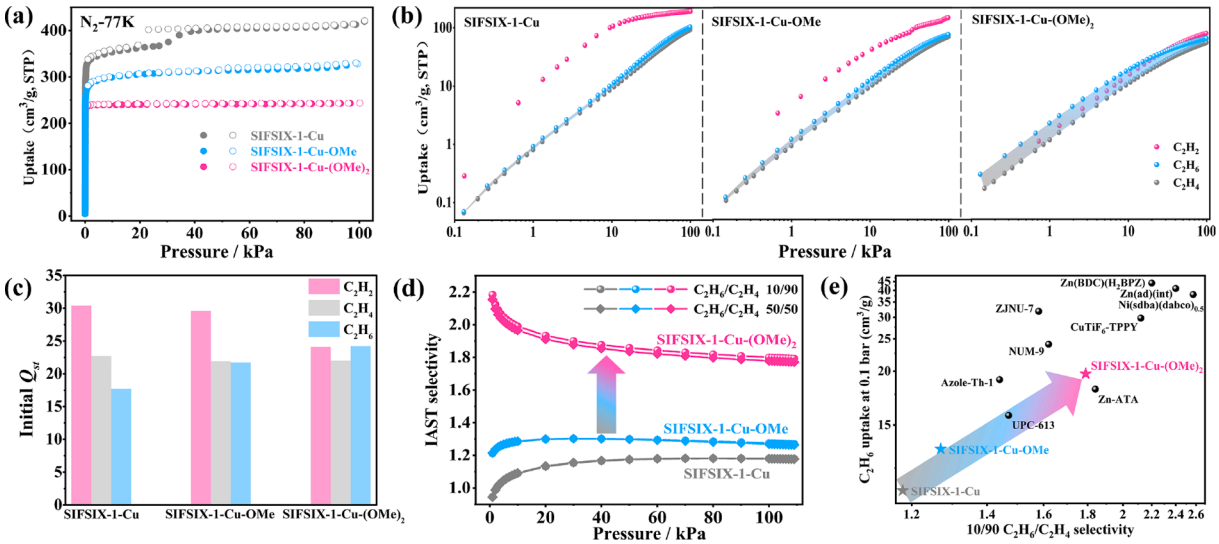

Fig. 2. Comparison of adsorption properties of **SIFSIX-1-Cu**, **SIFSIX-1-Cu-OMe** and **SIFSIX-1-Cu-(OMe)$_2$**. (a) N_2 adsorption isotherms at 77 K. (b) Gas adsorption isotherms of C_2H_2, C_2H_4 and C_2H_6 at 298 K. (c) Initial isosteric heat of adsorption (Q_{st}) of C_2H_2, C_2H_4, and C_2H_6. (d) The IAST selectivity of C_2H_6/C_2H_4 at 298 K. (e) Comparison of C_2H_6 uptake at 0.1 bar and 10/90 C_2H_6/C_2H_4 selectivity of these three materials and the reported famous MOFs that can realize one-step C_2H_4 purification from ternary C_2-gases mixture.

2. Experimental section

2.1. Materials synthesis

SIFSIX-1-Cu was prepared according to the reported literature [46]. An aqueous solution (3 mL) of $Cu(BF_4)_2{\cdot}6H_2O$ (1.00 mmol) and $(NH_4)_2{\cdot}SiF_6$ (1.00 mmol) was diffused to an ethylene glycol (3 mL) of 4,4′-bipyridine (2.00 mmol) in a rigid glass tube. After three days, purple single crystals were obtained.

An aqueous solution (3 mL) of $CuSiF_6$ (30 mg) was slowly diffused to a methanol (3 mL) of 3-methoxy-4,4′-bipyridine (20 mg) in a rigid glass tube. After a week, purple single crystals **SIFSIX-1-Cu-OMe** were obtained. Anal. Calcd (%) for the sample after adsorption: C, 36.59; H, 5.02; N, 7.76. Found: C, 37.12; H, 4.84; N, 7.75. It is observed that ca. eight water molecules are absorbed in activated **SIFSIX-1-Cu-OMe**.

An aqueous solution (3 mL) of $CuSiF_6$ (30 mg) was slowly diffused to a methanol (3 mL) of 3,3′-dimethoxy-4,4′-bipyridine (20 mg) in a rigid glass tube. After a week, purple single crystals **SIFSIX-1-Cu-(OMe)$_2$** were obtained. Anal. Calcd (%) for the sample after adsorption: C, 36.85; H, 5.15; N, 7.16. Found: C, 37.30; H, 4.92; N, 7.16. It is observed that ca. eight water molecules are absorbed in activated **SIFSIX-1-Cu-(OMe)$_2$**.

2.2. Gas sorption measurement

The gas adsorption isotherms were tested on a Micromeritics 3Flex surface area analyzer. Fresh samples were exchanged with ultra-dry methanol with a week. After that, **SIFSIX-1-Cu** was evacuated at room temperature for 24 h, **SIFSIX-1-Cu-OMe** and **SIFSIX-1-Cu-(OMe)$_2$** were activated by heating at 353 K for 10 h to completely remove the solvent molecules. The sorption curves of N_2 at 77 K, C_2H_2, C_2H_4 and C_2H_6 at different temperatures were collected in a liquid nitrogen bath, an ice-water bath and a water bath, respectively.

2.3. Breakthrough experiments

Dynamic breakthrough experiments were conducted on a homemade device. The activated sample, **SIFSIX-1-Cu** (1.2863 g), **SIFSIX-1-Cu-OMe** (0.8306 g) and **SIFSIX-1-Cu-(OMe)$_2$** (1.6648 g), were loaded into a stainless-steel column (4 mm internal diameter × 500 mm length), and a certain amount of silica wool was used to seal the end of the column. The columns were then activated with He gas (20 mL/min) at 60 ℃ (**SIFSIX-1-Cu**) or 80 ℃ (**SIFSIX-1-Cu-OMe** and **SIFSIX-1-Cu-(OMe)$_2$**) for 10 h. The gas mixture (C_2H_2/C_2H_4 = 1/99, *v/v*; C_2H_6/C_2H_4 = 10/90, *v/v*; $C_2H_2/C_2H_4/C_2H_6$ = 1/90/9, *v/v/v*) then flowed through the packed bed at a certain flow rate of 1 mL/min. The outlet gas was monitored by gas chromatography with a thermal conductivity detector (TCD). After a breakthrough experiment, samples were regenerated by purging with He gas (20 mL/min) at 60 ℃ (**SIFSIX-1-Cu**) or 80 ℃ (**SIFSIX-1-Cu-OMe** and **SIFSIX-1-Cu-(OMe)$_2$**) for 2 h.

3. Results and discussion

3.1. Structure analysis

SIFSIX-1-Cu, **SIFSIX-1-Cu-OMe** and **SIFSIX-1-Cu-(OMe)$_2$** were synthesized through diffusion using the corresponding pyridine ligand and $CuSiF_6$. Single-crystal X-ray diffraction (SCXRD) reveal that **SIFSIX-1-Cu-OMe** and **SIFSIX-1-Cu-(OMe)$_2$** possess isostructural structure with **SIFSIX-1-Cu**, which are in *P4/mmm* space group (Table S2). These compounds exhibit a two-dimensional (2D) *sql* layer constructed by the pyridine ligands and metal atoms, which are further connected by inorganic SiF_6^{2-} anionic to construct a 3D *pcu* pillar-layer framework with one-dimensional channels. As illustrated in Fig. 1, with the increase of the number of –OCH_3 groups, the pore size gradually decreases from 8.0 Å for **SIFSIX-1-Cu** to 7.3 Å for **SIFSIX-1-Cu-OMe** and further down to 6.3 Å for **SIFSIX-1-Cu-(OMe)$_2$**. More importantly, the incorporation of –OCH_3 groups within the pore walls of both **SIFSIX-1-Cu-OMe** and **SIFSIX-1-Cu-(OMe)$_2$** leads to a gradual increase in the number of O accessible sites compared to that of **SIFSIX-1-Cu**. Therefore, a suitable pore size combined with the presence of multiple supramolecular binding sites in the pore channel is expected to customize the pore environments that are more conducive to capturing C_2H_2 and C_2H_6, thereby achieving the one-step purification of C_2H_4 from a ternary mixture of $C_2H_2/C_2H_4/C_2H_6$.

3.2. Gas sorption measurements

The powder X-ray diffraction (PXRD) experiments indicate good phase purity of **SIFSIX-1-Cu**, **SIFSIX-1-Cu-OMe** and **SIFSIX-1-Cu-(OMe)$_2$** (Fig. S3). As shown in Figs. S4 and S5, the thermogravimetric analysis (TGA) and variable temperature (VT)-PXRD tests reveal that **SIFSIX-1-Cu-OMe** and **SIFSIX-1-Cu-(OMe)$_2$** exhibit exceptional

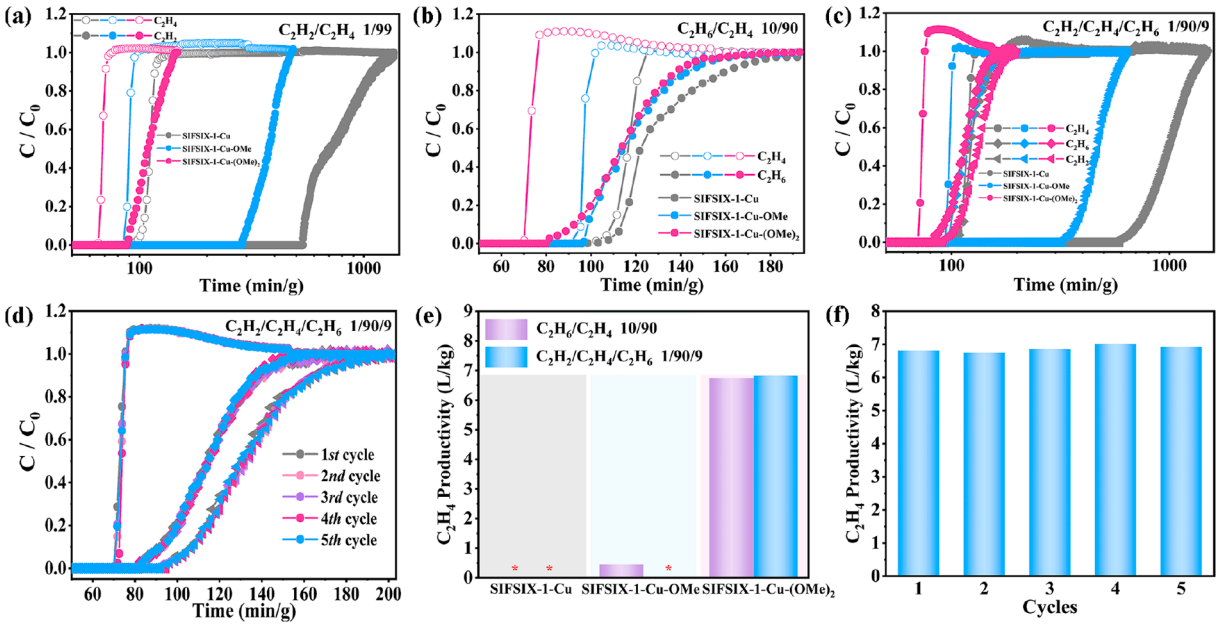

Fig. 3. Dynamic breakthrough experiments of **SIFSIX-1-Cu**, **SIFSIX-1-Cu-OMe** and **SIFSIX-1-Cu-(OMe)$_2$** at 298 K for (a) 1/99 C_2H_2/C_2H_4; (b) 10/90 C_2H_6/C_2H_4; (c) 1/90/9 $C_2H_2/C_2H_4/C_2H_6$. (d) Five cycles breakthrough experiments of **SIFSIX-1-Cu-(OMe)$_2$** for 1/90/9 $C_2H_2/C_2H_4/C_2H_6$. (e) Compare the C_2H_4 productivity calculated by binary C_2H_6/C_2H_4 (10/90) and ternary $C_2H_2/C_2H_4/C_2H_6$ (1/90/9) breakthrough experiments of the three materials. * represent that the material cannot achieve the one-step C_2H_4 purification. (f) The C_2H_4 productivity of multiple ternary $C_2H_2/C_2H_4/C_2H_6$ (1/90/9) cycles breakthrough experiments on **SIFSIX-1-Cu-(OMe)$_2$**.

thermal stability and can maintain their original structure at least to 453 K in air. Additionally, they demonstrate remarkable chemical stability (Fig. S6). Subsequently, the pore structure is examined by 77 K N_2 adsorption test. The experimental results demonstrate that the adsorption isotherms of three materials all exhibit the type-I curve, indicating their microporous characteristics (Fig. 2a). It is noteworthy that the corresponding Brunauer-Emmett-Teller (BET) surface area and pore volume gradually decrease from **SIFSIX-1-Cu** (1332 m^2/g, 0.65 cm^3/g) to **SIFSIX-1-Cu-OMe** (1130 m^2/g, 0.57 cm^3/g), and reach the value in **SIFSIX-1-Cu-(OMe)$_2$** (895 m^2/g, 0.38 cm^3/g). The pore size distribution obtained by density functional theory (DFT) is consistent with trend from the crystal structures (Fig. S7).

Single-component gas adsorption experiments of C_2H_2, C_2H_4 and C_2H_6 were conducted on **SIFSIX-1-Cu**, **SIFSIX-1-Cu-OMe** and **SIFSIX-1-Cu-(OMe)$_2$**. As shown in Fig. 2b, the maximum adsorption uptake of C_2H_2 is higher than that of C_2H_4 and C_2H_6 in all materials. Noteworthy, the difference of adsorption capacity for C_2H_6 and C_2H_4 is significantly increase from **SIFSIX-1-Cu** to **SIFSIX-1-Cu-OMe** and **SIFSIX-1-Cu-(OMe)$_2$**. At 298 K and 0.1 bar, the adsorption uptake of C_2H_6 (11.5 cm^3/g) is almost equal with C_2H_4 (9.8 cm^3/g) in **SIFSIX-1-Cu**, and the adsorption difference of C_2H_6 and C_2H_4 as well as the C_2H_6/C_2H_4 uptake ratio are only 1.7 cm^3/g and 117 %. In contrast, **SIFSIX-1-Cu-OMe** shows relatively higher C_2H_6 adsorption (13.5 cm^3/g) than C_2H_4 (10.4 cm^3/g), and the corresponding adsorption difference (3.1 cm^3/g) and uptake ratio of C_2H_6/C_2H_4 (130 %) are slightly larger than those of **SIFSIX-1-Cu**. As anticipated, **SIFSIX-1-Cu-(OMe)$_2$** exhibits extremely high adsorption amount of C_2H_6 (19.7 cm^3/g) at 298 K and 0.1 bar, about 1.7 times of **SIFSIX-1-Cu**, but only adsorbs C_2H_4 of 11.5 cm^3/g, resulting in the adsorption difference as high as 8.2 cm^3/g and an amazing C_2H_6/C_2H_4 uptake ratio of 171 % (Fig. S8). Moreover, such significant adsorption difference of C_2H_6 and C_2H_4 in **SIFSIX-1-Cu-(OMe)$_2$** can be maintained at multiple adsorption–desorption cycle experiments (Fig. S9).

Furthermore, the isosteric heats of adsorption (Q_{st}) of C_2H_2, C_2H_4 and C_2H_6 are calculated based on the Virial equation to investigate the interaction between the framework and gas molecules (Figs. S12-S14). As shown in Fig. 2c, the initial Q_{st} of C_2H_2 is larger than that of C_2H_4 in all materials. Noteworthy, in **SIFSIX-1-Cu**, the initial Q_{st} of C_2H_4 (22.7 kJ/mol) is higher than that of C_2H_6 (17.7 kJ/mol), and the difference of isosteric adsorption heats (ΔQ_{st}) is 5.0 kJ/mol. For **SIFSIX-1-Cu-OMe**, although the Q_{st} order is the same as that of **SIFSIX-1-Cu**, in which C_2H_4 (21.9 kJ/mol) is higher than C_2H_6 (21.7 kJ/mol), the ΔQ_{st} is significantly reduced to 0.2 kJ/mol. As anticipated, **SIFSIX-1-Cu-(OMe)$_2$** shows a inversed Q_{st} order of C_2H_6 (24.2 kJ/mol) > C_2H_4 (22.0 kJ/mol) with a high difference (2.2 kJ/mol), indicating that **SIFSIX-1-Cu-(OMe)$_2$** has stronger affinity for C_2H_6 than that for C_2H_4.

Subsequently, we evaluate the separation potential of these materials through IAST selectivity. As expected, all three materials show outstanding IAST selectivity of C_2H_2/C_2H_4 mixture (Fig. S15). Regarding different ratios of C_2H_6/C_2H_4 mixture, the order of C_2H_6/C_2H_4 selectivity is **SIFSIX-1-Cu-(OMe)$_2$** > **SIFSIX-1-Cu-OMe** > **SIFSIX-1-Cu** (Fig. 2d). Especially, the 10/90 C_2H_6/C_2H_4 IAST selectivity is significantly improve from 1.18 (**SIFSIX-1-Cu**) to 1.27 (**SIFSIX-1-Cu-OMe**), and finally reach a remarkably high value of 1.79 (**SIFSIX-1-Cu-(OMe)$_2$**). As indicated in Fig. 2e, both C_2H_6 adsorption capacity at 298 K and 0.1 bar and 10/90 C_2H_6/C_2H_4 IAST selectivity gradually increase from **SIFSIX-1-Cu** (11.5 cm^3/g, 1.18) to **SIFSIX-1-Cu-OMe** (13.5 cm^3/g, 1.27), and reach the maximum in **SIFSIX-1-Cu-(OMe)$_2$** (19.7 cm^3/g, 1.79), which is also higher than some state-of-the-art materials capable of one-step purification of C_2H_4 from three-component C_2 hydrocarbon mixture, such as Azole-Th-1 (19.0 cm^3/g, 1.44) [47] and UPC-613 (15.7 cm^3/g, 1.47) [48], but lower than $CuTiF_6$-TPPY (29.8 cm^3/g, 2.12) [40] and Ni(sdba)(dabco)$_{0.5}$ (38.1 cm^3/g, 2.57) [49]. Based on the above results, by modifying one or two –OCH_3 groups into **SIFSIX-1-Cu**, the C_2H_6 adsorption capacity, C_2H_6/C_2H_4 uptake ratio and C_2H_6/C_2H_4 IAST selectivity could be stepwise improved. Therefore, **SIFSIX-1-Cu-(OMe)$_2$** may serve as a promising adsorbent that enables one-step purification of C_2H_4 from ternary $C_2H_2/C_2H_4/C_2H_6$ mixture.

3.3. Dynamic breakthrough experiments

To evaluate the actual separation performance, dynamic breakthrough experiments were performed on **SIFSIX-1-Cu**, **SIFSIX-1-Cu-OMe** and **SIFSIX-1-Cu-(OMe)$_2$**. As anticipated, all three materials can

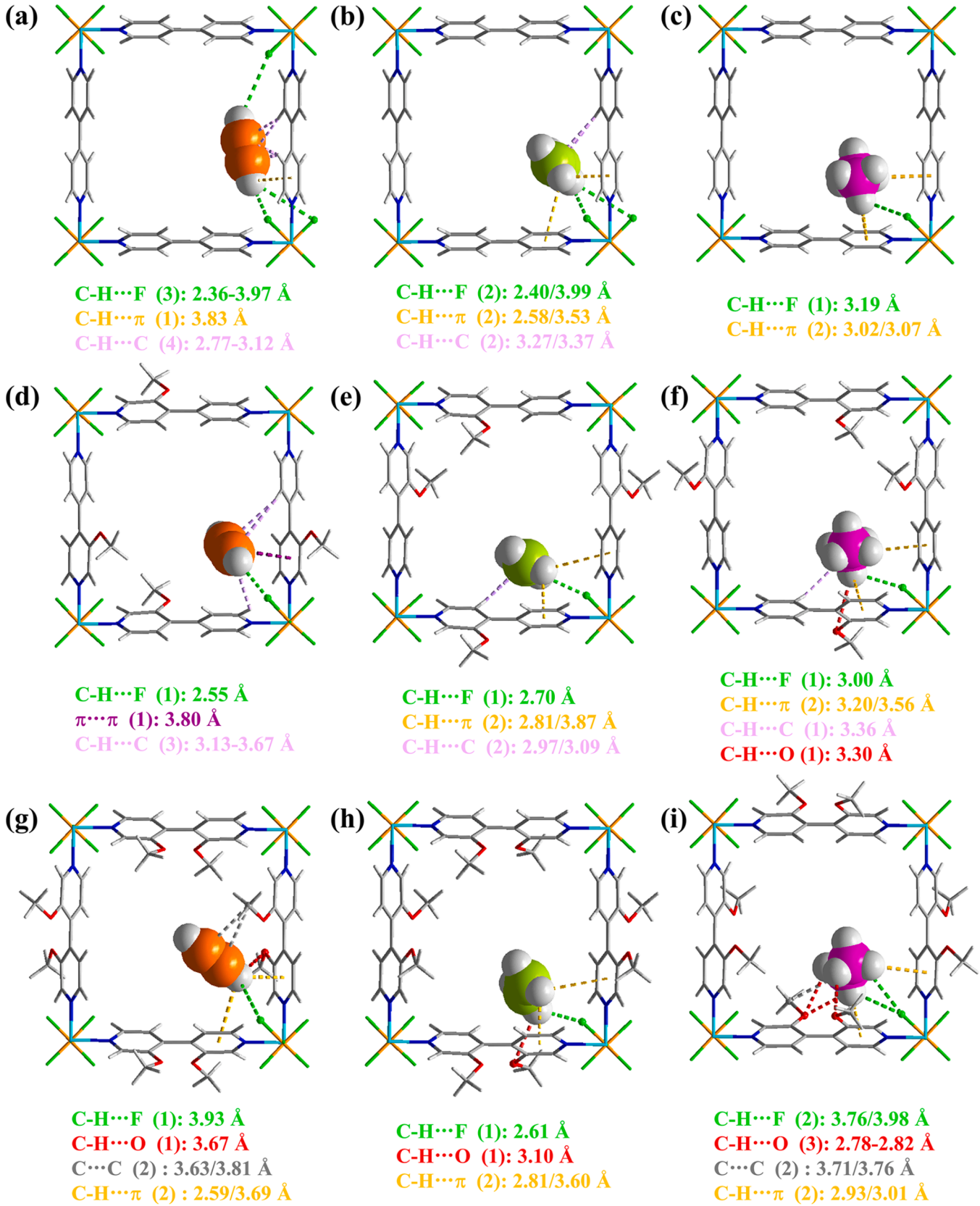

Fig. 4. The optimal gas adsorption sites by GCMC simulations. (a) C_2H_2; (b) C_2H_4; (c) C_2H_6 in **SIFSIX-1-Cu**. (d) C_2H_2; (e) C_2H_4; (f) C_2H_6 in **SIFSIX-1-Cu-OMe**. (g) C_2H_2; (h) C_2H_4; (i) C_2H_6 in **SIFSIX-1-Cu-(OMe)$_2$**.

efficiently separate C_2H_2/C_2H_4 (1/99) mixture. C_2H_4 breaks out first and C_2H_2 is also detected after a considerable time interval, suggesting that the framework has stronger interactions with C_2H_2 than C_2H_4 (Fig. 3a). Furthermore, a binary gas mixture of C_2H_6/C_2H_4 (10/90) was tested. As shown in Fig. 3b, C_2H_4 and C_2H_6 break out almost simultaneously and the purification of C_2H_4 cannot be achieved with **SIFSIX-1-Cu**. Meanwhile, for **SIFSIX-1-Cu-OMe**, C_2H_4 is detected at about 91 min and C_2H_6 flows at 97 min. However, only 0.45 L/kg of polymer-grade C_2H_4 (≥99.95 %) can be obtained. As anticipated, compared with **SIFSIX-1-Cu** and **SIFSIX-1-Cu-OMe**, the breakthrough time interval between C_2H_4 and C_2H_6 is sharply increase to 11 min in **SIFSIX-1-Cu-(OMe)$_2$**, and the polymer-grade C_2H_4 (≥99.95 %) productivity is up to 6.75 L/kg, which is nearly 15 times higher than that of **SIFSIX-1-Cu-OMe** (Fig. 3e). Furthermore, we investigated the separation ability of these three materials in ternary $C_2H_2/C_2H_4/C_2H_6$ (1/90/9) mixture. The experimental results show that C_2H_2 has the longest retention time on the breakthrough column in all materials, while **SIFSIX-1-Cu** and **SIFSIX-1-Cu-OMe** cannot realize one-step C_2H_4 purification from ternary gas mixture due to the simultaneous outflow of C_2H_4 and C_2H_6. In contrast, for **SIFSIX-1-Cu-(OMe)$_2$**, C_2H_4 is detected at 68 min, while C_2H_6 is not detected at outlet until 82 min, and the polymer-grade C_2H_4 (≥99.95 %) productivity is as high as 6.82 L/kg (Fig. 3c and 3e). The C_2H_4 productivity of **SIFSIX-1-Cu-(OMe)$_2$** is superior to some reported materials that can achieve C_2H_4 purification from $C_2H_2/C_2H_4/C_2H_6$ (1/90/9) mixture, such as UiO-66-CF_3 (3.49 L/kg) [50], LIFM-XYY-6 (3.20 L/kg) [28] and HIAM-210 (2.56 L/kg) [51]. Since the stability of material is crucial in practical industrial application, we further performed multiple cycle breakthrough experiments on **SIFSIX-1-Cu-(OMe)$_2$**. As indicated in Fig. 3d and 3f, the separation performance and the polymer-grade C_2H_4 (≥99.95 %) productivity from $C_2H_2/C_2H_4/C_2H_6$ (1/90/9) remain basically unchanged after five cycles, which shows the excellent recyclability of **SIFSIX-1-Cu-(OMe)$_2$**. In summary, compared to **SIFSIX-1-Cu** and **SIFSIX-1-Cu-OMe**, **SIFSIX-1-Cu-(OMe)$_2$** shows exceptional separation performance and ultra-high stability through the pore environment engineering, making it a potential material for purifying C_2H_4 from ternary C_2-gases mixtures in one step.

3.4. Theoretical calculations

The optimal adsorption sites of C_2H_2, C_2H_4 and C_2H_6 on the three materials were determined by grand canonical monte carlo (GCMC) simulations, and the binding energies were evaluated based on dispersion-corrected density functional theory (DFT) calculations [52,53]. As shown in Fig. 4a-4c, in **SIFSIX-1-Cu**, we can clearly find that both C_2H_2 and C_2H_4 can form multiple C-H…F interactions, C-H…π interactions and C-H…C interactions with the framework, whereas only one C-H…F interaction and two C-H…π interactions can be noted for C_2H_6, The calculated static binding energies of three gases follow the tendency of C_2H_2 (−69.98 kJ/mol) > C_2H_4 (−51.36 kJ/mol) > C_2H_6 (−35.71 kJ/mol). After modification of the ligand with one –OCH_3 group, for C_2H_6, in addition to one C-H…F interaction, two C-H…π interactions and one C-H…C interaction with the pore surface, it can also form an additional C-H…O interaction with the –OCH_3 group compared with C_2H_2 and C_2H_4 (Fig. 4d-4f). The binding energy of C_2H_6 increases to −45.56 kJ/mol, but remains lower than that of C_2H_2 (−61.02 kJ/mol) and C_2H_4 (−49.28 kJ/mol). When the number of –OCH_3 group is increased to two, as anticipated, C_2H_6 not only forms two C-H…F interactions and two C-H…π interactions with the skeleton, but also forms extra three C-H…O interactions and two C…C interactions with the inserted –OCH_3 groups. It can be observed that increasing the number of –OCH_3 groups in the pore wall leads to more supramolecular interactions, especially C-H…O interactions, between C_2H_6 and the pore surface. In contrast, only one C-H…O interaction is produced between the introduced –OCH_3 groups and C_2H_4 (Fig. 4g-4i). Therefore, in **SIFSIX-1-Cu-(OMe)$_2$**, the insertion of –OCH_3 group results in more supramolecular interactions between C_2H_6 and the framework than C_2H_4, with the binding energy of C_2H_6 (−45.52 kJ/mol) > C_2H_2 (−43.27 kJ/mol) > C_2H_4 (−41.62 kJ/mol). The above results demonstrate that an optimal pore environment is tailored for **SIFSIX-1-Cu-(OMe)$_2$** through the synergistic effect of reduction in pore size and increase in O binding sites, which endow enhancing affinity towards C_2H_6 compared with C_2H_4. Therefore, **SIFSIX-1-Cu-(OMe)$_2$** realizes efficient one-step purification of C_2H_4 from a ternary $C_2H_2/C_2H_4/C_2H_6$ mixture.

4. Conclusions

In conclusion, we have successfully customized the pore environments of C_2H_2-selective materials through ligand functionalization to achieve one-step purification of C_2H_4 from a ternary $C_2H_2/C_2H_4/C_2H_6$ mixture. The O binding sites are continuously increased by stepwise modifying one and two –OCH_3 groups into C_2H_2-selective **SIFSIX-1-Cu**, resulting in significant improvements in the adsorption capacity of C_2H_6, the C_2H_6/C_2H_4 uptake ratio, as well as the C_2H_6/C_2H_4 IAST selectivity. Moreover, in comparison to **SIFSIX-1-Cu** and **SIFSIX-1-Cu-OMe**, which are incapable of achieving the purification of C_2H_4 from ternary C_2-hydrocarbons, **SIFSIX-1-Cu-(OMe)$_2$** can realize the one-step acquisition of polymer-grade C_2H_4 from a mixture of $C_2H_2/C_2H_4/C_2H_6$ (1/90/9) with significantly high productivity of 6.82 L/kg. Theoretical calculations further demonstrate that the pore surface of **SIFSIX-1-Cu-(OMe)$_2$** possesses multiple binding sites for C_2H_6, in contrast to C_2H_4. Consequently, **SIFSIX-1-Cu-(OMe)$_2$** exhibits good performance in purifying C_2H_4 from a mixture of $C_2H_2/C_2H_4/C_2H_6$. The present work represents a significant advancement in stepwise customizing pore environments on a C_2H_2-selective material, aiming to achieve one-step C_2H_4 purification from ternary C_2 hydrocarbon mixtures. This work provides novel insights into the development of C_2H_2/C_2H_6-selective MOFs for one-step acquisition of C_2H_4 from C_2-hydrocarbons.

CRediT authorship contribution statement

Shuixiang Zou: Conceptualization, Methodology, Software, Writing – original draft. **Cheng Chen:** Supervision, Writing – review & editing. **Zhengyi Di:** Supervision, Writing – review & editing. **Yuanzheng Liu:** Supervision, Writing – review & editing. **Hengbo Li:** Supervision, Writing – review & editing. **Yashuang Li:** Supervision, Writing – review & editing. **Rajamani Krishna:** Software, Supervision, Writing – review & editing. **Daqiang Yuan:** Software, Supervision, Writing – review & editing. **Mingyan Wu:** Resources, Funding acquisition, Supervision, Writing – review & editing.

Declaration of competing interest

The authors declare that they have no known competing financial interests or personal relationships that could have appeared to influence the work reported in this paper.

Data availability

Data will be made available on request.

Acknowledgements

This work is supported by NSFC (22271282) and the Self-deployment Project Research Program of Haixi Institutes, Chinese Academy of Sciences with the grant number of CXZX-2022-JQ04. Additionally, this work is also supported by Fujian Science & Technology Innovation Laboratory for Optoelectronic Information of China (No. 2021ZR120) and NSF of Fujian Province (No. 2021 J01517 and 2020 J06034).

Appendix A. Supplementary data

Supplementary data to this article can be found online at https://doi.org/10.1016/j.seppur.2024.129358.

References

[1] I. Amghizar, L. Vandewalle, K. Van Geem, G. Marin, New trends in olefin production, Engineering 3 (2017) 171–178.

[2] H. Li, C. Chen, Q. Li, X.J. Kong, Y. Liu, Z. Ji, S. Zou, M. Hong, M. Wu, An ultrastable supramolecular framework based on consecutive side-by-side hydrogen bonds for one-step C_2H_4/C_2H_6 separation, Angew. Chem. Int. Ed. 63 (2024) e202401754.

[3] Q. Wang, D. Ning, H. Chen, Y. Chen, J. Li, L. Li, Enhanced ethane/ethylene separation based on metal regulation in zeolitic imidazolate frameworks, Chin. J. Struct. Chem. 42 (2023) 100147.

[4] Y. Duan, Y. Huang, C. Wang, Q. Wang, K. Ge, Z. Lu, H. Wang, J. Duan, J. Bai, W. Jin, Formation and fine-tuning of metal-organic frameworks with carboxylic pincers for the recognition of a C_2H_2 tetramer and highly selective separation of C_2H_2/C_2H_4, Chem. Sci. 14 (2023) 4605–4611.

[5] T. Ren, M. Patel, K. Blok, Olefins from conventional and heavy feedstocks: Energy use in steam cracking and alternative processes, Energy 31 (2006) 425–451.

[6] M. Fakhroleslam, S. Sadrameli, Thermal/catalytic cracking of liquid hydrocarbons for the production of olefins: A state-of-the-art review II: Catalytic cracking review, Fuel 252 (2019) 553–566.

[7] D.S. Sholl, R.P. Lively, Seven chemical separations to change the world, Nature 532 (2016) 435–437.

[8] Y. Han, L. Meng, Y. Liu, H. Li, Z. Ji, Y. Zhou, M. Wu, Z. Han, Expanding nonpolar pore surfaces in stable ethane-selective MOF to boost ethane/ethylene separation performance, Sep. Purif. Technol. 315 (2023) 123642.

[9] Y. Yang, L. Li, R.-B. Lin, Y. Ye, Z. Yao, L. Yang, F. Xiang, S. Chen, Z. Zhang, S. Xiang, B. Chen, Ethylene/ethane separation in a stable hydrogen-bonded organic framework through a gating mechanism, Nat. Chem. 13 (2021) 933–939.

[10] Y. Liu, J. Liu, H. Xiong, J. Chen, S. Chen, Z. Zeng, S. Deng, Negative electrostatic potentials in a hofmann-type metal-organic framework for efficient acetylene separation, Nat. Commun. 13 (2022) 5515.

[11] J. Tian, Q. Chen, F. Jiang, D. Yuan, M. Hong, Optimizing acetylene sorption through induced-fit transformations in a chemically stable microporous framework, Angew. Chem. Int. Ed. 62 (2023) e202215253.

[12] J.-W. Wang, S.-C. Fan, H.-P. Li, X. Bu, Y.-Y. Xue, Q.-G. Zhai, De-linker-enabled exceptional volumetric acetylene storage capacity and benchmark C_2H_2/C_2H_4 and C_2H_2/CO_2 separations in metal-organic frameworks, Angew. Chem. Int. Ed. 62 (2023) e202217839.

[13] X. Mu, Y. Xue, M. Hu, P. Zhang, Y. Wang, H. Li, S. Li, Q. Zhai, Fine-tuning of pore-space-partitioned metal-organic frameworks for efficient C_2H_2/C_2H_4 and C_2H_2/CO_2 separation, Chin. Chem. Lett. 34 (2023) 107296.

[14] K. Jiang, Y. Gao, P. Zhang, S. Lin, L. Zhang, A new perchlorate-based hybrid ultramicroporous material with rich bare oxygen atoms for high C_2H_2/CO_2 separation, Chin. Chem. Lett. 34 (2023) 108039.

[15] Z. Bao, J. Wang, Z. Zhang, H. Xing, Q. Yang, Y. Yang, H. Wu, R. Krishna, W. Zhou, B. Chen, Q. Ren, Molecular sieving of ethane from ethylene through the molecular cross-section size differentiation in gallate-based metal-organic frameworks, Angew. Chem. Int. Ed. 57 (2018) 16020–16025.

[16] R.-B. Lin, L. Li, H.-L. Zhou, H. Wu, C. He, S. Li, R. Krishna, J. Li, W. Zhou, B. Chen, Molecular sieving of ethylene from ethane using a rigid metal-organic framework, Nat. Mater. 17 (2018) 1128.

[17] Q. Ding, Z. Zhang, C. Yu, P. Zhang, J. Wang, X. Cui, C.-H. He, S. Deng, H. Xing, Exploiting equilibrium-kinetic synergetic effect for separation of ethylene and ethane in a microporous metal-organic framework, Sci. Adv. 6 (2020) eaaz4322.

[18] Z. Di, X. Zheng, Y. Qi, H. Yuan, C.-P. Li, Recent advances in C_2 gases separation and purification by metal-organic frameworks, Chin. J. Struct. Chem. 41 (2022) 2211031–2211044.

[19] J.-R. Li, R. Kuppler, H.-C. Zhou, Selective gas adsorption and separation in metal-organic frameworks, Chem. Soc. Rev. 38 (2009) 1477–1504.

[20] L. Wang, H. Huang, X. Zhang, H. Zhao, F. Li, Y. Gu, Designed metal-organic frameworks with potential for multi-component hydrocarbon separation, Coord. Chem. Rev. 484 (2023) 215111.

[21] H.-G. Hao, Y.-F. Zhao, D.-M. Chen, J.-M. Yu, K. Tan, S. Ma, Y. Chabal, Z.-M. Zhang, J.-M. Dou, Z.-H. Xiao, G. Day, H.-C. Zhou, T.-B. Lu, Simultaneous trapping of C_2H_2 and C_2H_6 from a ternary mixture of $C_2H_2/C_2H_4/C_2H_6$ in a robust metal-organic framework for the purification of C_2H_4, Angew. Chem. Int. Ed. 57 (2018) 16067–16071.

[22] Q. Ding, Z. Zhang, Y. Liu, C. Kungang, R. Krishna, S. Zhang, One-step ethylene purification from ternary mixtures in a metal-organic framework with customized pore chemistry and shape, Angew. Chem. Int. Ed. 61 (2022) e202208134.

[23] Q. Ding, Z. Zhang, P. Zhang, C. Yu, C.-H. He, X. Cui, H. Xing, One-step ethylene purification from ternary mixture by synergetic molecular shape and size matching in a honeycomb-like ultramicroporous material, Chem. Eng. J. 450 (2022) 138272.

[24] G.-D. Wang, Y.-Z. Li, W.-J. Shi, L. Hou, Y.-Y. Wang, Z. Zhu, One-step C_2H_4 purification from ternary $C_2H_6/C_2H_4/C_2H_2$ mixtures by a robust metal-organic framework with customized pore environment, Angew. Chem. Int. Ed. 61 (2022) e202205427.

[25] H.-M. Wen, C. Yu, M. Liu, C. Lin, B. Zhao, H. Wu, W. Zhou, B. Chen, J. Hu, Construction of negative electrostatic pore environments in a scalable, stable and low-cost metal-organic framework for one-step ethylene purification from ternary mixtures, Angew. Chem. Int. Ed. 62 (2023) e202309108.

[26] S. Xian, J. Peng, H. Pandey, W. Graham, L. Yu, H. Wang, K. Tan, T. Thonhauser, J. Li, Simultaneous removal of C_2H_2 and C_2H_6 for C_2H_4 purification by robust MOFs featuring high density of heteroatoms, J. Mater. Chem. A 11 (2023) 21401–21410.

[27] X.W. Gu, J.X. Wang, E. Wu, H. Wu, W. Zhou, G. Qian, B. Chen, B. Li, Immobilization of lewis basic sites into a stable ethane-selective MOF enabling one-step separation of ethylene from a ternary mixture, J. Am. Chem. Soc. 144 (2022) 2614–2623.

[28] Y. Xiong, C.-X. Chen, T. Pham, Z.-W. Wei, K. Forrest, M. Pan, C.-Y. Su, Dynamic spacer installation of multifunctionalities into metal-organic frameworks for spontaneous one-step ethylene purification from a ternary C_2-hydrocarbons mixture, CCS Chem. 6 (2023) 241–254.

[29] C. Song, F. Zheng, Y. Liu, Q. Yang, Z. Zhang, Q. Ren, Z. Bao, Spatial distribution of nitrogen binding sites in metal-organic frameworks for selective ethane adsorption and one-step ethylene purification, Angew. Chem. Int. Ed. 62 (2023) e202313855.

[30] X. Cui, K. Chen, H. Xing, Q. Yang, R. Krishna, Z. Bao, H. Wu, W. Zhou, X. Dong, Y. Han, B. Li, Q. Ren, M.J. Zaworotko, B. Chen, Pore chemistry and size control in hybrid porous materials for acetylene capture from ethylene, Science 353 (2016) 141–144.

[31] B. Li, X. Cui, D. O'Nolan, H.M. Wen, M. Jiang, R. Krishna, H. Wu, R.B. Lin, Y. S. Chen, D. Yuan, H. Xing, W. Zhou, Q. Ren, G. Qian, M.J. Zaworotko, B. Chen, An ideal molecular sieve for acetylene removal from ethylene with record selectivity and productivity, Adv. Mater. 29 (2017) 1704210.

[32] T. Ke, Q. Wang, J. Shen, J. Zhou, Z. Bao, Q. Yang, Q. Ren, Molecular sieving of C_2–C_3 alkene from alkyne with tuned threshold pressure in robust layered metal-organic frameworks, Angew. Chem. Int. Ed. 59 (2020) 12725–12730.

[33] Q.-L. Qian, X.-W. Gu, J. Pei, H.-M. Wen, H. Wu, W. Zhou, B. Li, G. Qian, A novel anion-pillared metal-organic framework for highly efficient separation of acetylene from ethylene and carbon dioxide, J. Mater. Chem. A 9 (2021) 9248–9255.

[34] X.-W. Gu, E. Wu, J.-X. Wang, H.-M. Wen, B. Chen, B. Li, G. Qian, Programmed fluorine binding engineering in anion-pillared metal-organic framework for record trace acetylene capture from ethylene, Sci. Adv. 9 (2023) eadh0135.

[35] J. Shen, X. He, T. Ke, R. Krishna, J. Baten, R. Chen, Z. Bao, H. Xing, M. Dincă, Z. Zhang, Q. Yang, Q. Ren, Simultaneous interlayer and intralayer space control in two-dimensional metal-organic frameworks for acetylene/ethylene separation, Nat. Commun. 11 (2020) 1–10.

[36] J. Wang, Y. Zhang, P. Zhang, J. Hu, R.-B. Lin, Q. Deng, Z. Zeng, H. Xing, S. Deng, B. Chen, Optimizing pore space for flexible-robust metal-organic framework to boost trace acetylene removal, J. Am. Chem. Soc. 142 (2020) 9744–9751.

[37] J. Wang, Y. Zhang, Y. Su, X. Liu, P. Zhang, R.-B. Lin, S. Chen, Q. Deng, Z. Zeng, S. Deng, B. Chen, Fine pore engineering in a series of isoreticular metal-organic frameworks for efficient C_2H_2/CO_2 separation, Nat. Commun. 13 (2022) 200.

[38] L. Li, H.M. Wen, C. He, R.B. Lin, R. Krishna, H. Wu, W. Zhou, J. Li, B. Li, B. Chen, A metal-organic framework with suitable pore size and specific functional sites for the removal of trace propyne from propylene, Angew. Chem. Int. Ed. 57 (2018) 15183–15188.

[39] L. Yang, X. Cui, Z. Zhang, Q. Yang, Z. Bao, Q. Ren, H. Xing, An asymmetric anion-pillared metal-organic framework as a multisite adsorbent enables simultaneous removal of propyne and propadiene from propylene, Angew. Chem. Int. Ed. 57 (2018) 13145–13149.

[40] P. Zhang, Y. Zhong, Y. Zhang, Z. Zhu, Y. Liu, Y. Su, J. Chen, S. Chen, Z. Zeng, H. Xing, S. Deng, J. Wang, Synergistic binding sites in a hybrid ultramicroporous material for one-step ethylene purification from ternary C_2 hydrocarbon mixtures, Sci. Adv. 8 (2022) eabn9231.

[41] L. Li, R.-B. Lin, R. Krishna, H. Li, S. Xiang, H. Wu, J. Li, W. Zhou, B. Chen, Ethane/ethylene separation in a metal-organic framework with iron-peroxo sites, Science 362 (2018) 443–446.

[42] C.X. Chen, Z.W. Wei, T. Pham, P.C. Lan, L. Zhang, K.A. Forrest, S. Chen, A.M. Al-Enizi, A. Nafady, C.Y. Su, S. Ma, Nanospace engineering of metal-organic frameworks through dynamic spacer installation of multifunctionalities for efficient separation of ethane from ethane/ethylene mixtures, Angew. Chem. Int. Ed. 60 (2021) 9680–9685.

[43] Z. Di, C. Liu, J. Pang, S. Zou, Z. Ji, F. Hu, C. Chen, D. Yuan, M. Hong, M. Wu, A metal-organic framework with nonpolar pore surfaces for the one-step acquisition of C_2H_4 from a C_2H_4 and C_2H_6 mixture, Angew. Chem. Int. Ed. 61 (2022) e202210343.

[44] G.-D. Wang, R. Krishna, Y.-Z. Li, W.-J. Shi, L. Hou, Y.-Y. Wang, Z. Zhu, Boosting ethane/ethylene separation by MOFs through the amino-functionalization of pores, Angew. Chem. Int. Ed. 61 (2022) e202213015.

[45] Y. Ye, Y. Xie, Y. Shi, L. Gong, J. Phipps, A. Al-Enizi, A. Nafady, B. Chen, S. Ma, A microporous metal-organic framework with unique aromatic pore surfaces for high performance C_2H_6/C_2H_4 separation, Angew. Chem. Int. Ed. 62 (2023) e202302564.

[46] S. Noro, S. Kitagawa, M. Kondo, K. Seki, A new, methane adsorbent, porous coordination polymer $[\{CuSiF_6(4,4'\text{-bipyridine})_2\}_n]$, Angew. Chem. Int. Ed. 39 (2000) 2082–2084.

[47] Z. Xu, X. Xiong, J. Xiong, R. Krishna, L. Li, Y. Fan, F. Luo, B. Chen, A robust Th-azole framework for highly efficient purification of C_2H_4 from a $C_2H_4/C_2H_2/C_2H_6$ mixture, Nat. Commun. 11 (2020) 3163.

[48] Y. Wang, C. Hao, W. Fan, M. Fu, X. Wang, Z. Wang, L. Zhu, Y. Li, X. Lu, F. Dai, Z. Kang, R. Wang, W. Guo, S. Hu, D. Sun, One-step ethylene purification from an acetylene/ethylene/ethane ternary mixture by cyclopentadiene cobalt-functionalized metal-organic frameworks, Angew. Chem. Int. Ed. 60 (2021) 11350–11358.

[49] H. Shuai, J. Liu, Y. Teng, X. Liu, L. Wang, H. Xiong, P. Wang, J. Chen, S. Chen, Z. Zhou, S. Deng, Pillar-layered metal-organic frameworks with benchmark C_2H_2/C_2H_4 and C_2H_6/C_2H_4 selectivity for one-step C_2H_4 production, Sep. Purif. Technol. 323 (2023) 124392.
[50] J. Liu, J. Miao, H. Wang, Y. Gai, J. Li, Enhanced one-step purification of C_2H_4 from $C_2H_2/C_2H_4/C_2H_6$ mixtures by fluorinated Zr-MOF, AIChE J. 69 (2023) e18021.
[51] J. Liu, H. Wang, J. Li, Pillar-layer Zn-triazolate-dicarboxylate frameworks with a customized pore structure for efficient ethylene purification from ethylene/ethane/acetylene ternary mixtures, Chem. Sci. 14 (2023) 5912–5917.
[52] T.D. Kuehne, M. Iannuzzi, M. Del Ben, V.V. Rybkin, P. Seewald, F. Stein, T. Laino, R.Z. Khaliullin, O. Schutt, F. Schiffmann, D. Golze, J. Wilhelm, S. Chulkov, M. H. Bani-Hashemian, V. Weber, U. Borstnik, M. Taillefumier, A.S. Jakobovits, A. Lazzaro, H. Pabst, T. Mueller, R. Schade, M. Guidon, S. Andermatt, N. Holmberg, G.K. Schenter, A. Hehn, A. Bussy, F. Belleflamme, G. Tabacchi, A. Gloss, M. Lass, I. Bethune, C.J. Mundy, C. Plessl, M. Watkins, J. VandeVondele, M. Krack, J. Hutter, CP2K: An electronic structure and molecular dynamics software package-quickstep: Efficient and accurate electronic structure calculations, J. Chem. Phys. 152 (2020) 194103.
[53] T. Lu, F. Chen, Multiwfn: A multifunctional wavefunction analyzer, J. Comput. Chem. 33 (2012) 580–592.

Supplementary Information

Stepwise customizing pore environments of C_2H_2-selective frameworks for one-step C_2H_4 acquisition from ternary mixtures

Shuixiang Zou[a,b], Cheng Chen[a], Zhengyi Di[a], Yuanzheng Liu[a], Hengbo Li[a], Yashuang Li[a], Rajamani Krishna[c], Daqiang Yuan[a], Mingyan Wu[a,b,*]

[a]*State Key Lab of Structural Chemistry, Fujian Institute of Research on the Structure of Matter, Chinese Academy of Sciences, Fuzhou, Fujian 350002, China*

[b]*University of Chinese Academy of Sciences, Beijing, 100049, China*

[c]*Van't Hoff Institute for Molecular Sciences, University of Amsterdam, Science Park 904, 1098 XH Amsterdam, The Netherlands*

*Corresponding author.

E-mail: wumy@fjirsm.ac.cn

Materials and Instrumentation

The ligand of 3-methoxy-4,4′-bipyridine (Bpy-OMe) and 3,3′-dimethoxy-4,4′-bipyridine (Bpy-$(OMe)_2$) were synthesized according to the methods reported in the literature [1]. All reagents were purchased from commercial sources and used without further purification. Powder X-ray diffraction (PXRD) and Variable-Temperature (VT)-PXRD data were collected using a Rigaku MiniFlex600 X-ray diffractometer with Cu-Kα (λ = 0.154 nm). Thermogravimetric analysis (TGA) was conducted on an NETZSCH STA 449C unit at heating rate of 10 ºC/min under a nitrogen atmosphere from room temperature to 900 ºC. Elemental analyses for C, H, and N were carried out on a Elementar Vario MICRO elemental analyzer.

Single-Crystal X-ray Crystallography

Single crystal data was collected on a XtaLAB Synergy R, HyPix diffractometer equipped with Cu-Kα radiation (λ = 1.54184 Å). The structure was solved by the intrinsic method of Olex2 and meanwhile refined by the full-matrix least-squares technique on F^2 using the SHELX program. The *SQUEEZE* command in *PLATON* was employed to eliminate the highly diffused electron density in the channels. Crystallography data and other details were listed in Table S2.

Calculation of the isosteric heat of adsorption (Q_{st})

The isosteric enthalpies of adsorption for C_2H_2, C_2H_4 and C_2H_6 were calculated using the single component gas adsorption isotherms at 273 K and 298 K based on the Virial equation.

$$\ln P = \ln N + \frac{1}{T}\sum_{i=0}^{m} a_i N^i + \sum_{i=0}^{n} b_i N^i \quad (1)$$

$$Q_{st} = -R\sum_{i=0}^{m} a_i N^i \quad (2)$$

P is pressure (mmHg), N is the adsorbed capacity (mmol g^{-1}), T is the temperature (K), R is the gas constant (8.314 J K^{-1} mol^{-1}), a_i and b_i are virial coefficients, m and n are the number of coefficients.

Calculation of IAST selectivity

Single component gas adsorption isotherms were fitted with single-site Langmuir–Freundlich model:

$$N = A\frac{bp^c}{1+bp^c} \quad (2)$$

N is adsorbed capacity (mmol g^{-1}), A is the saturation adsorption capacity (mmol g^{-1}), b is the Langmuir constant, c is the Freundlich exponent.

The resulting fitting parameters of A, b and c were used to calculate IAST selectivity:

$$S_{\frac{1}{2}} = \left(\frac{x_1}{x_2}\right)\left(\frac{y_2}{y_1}\right) \quad (3)$$

x and y are the molar fractions in the adsorbed phase and bulk phase, respectively.

Transient Breakthrough Simulations

Single component Transient breakthrough experiments were carried out for ternary 1/90/9 C_2H_2(1)/C_2H_4(2)/C_2H_6(3) mixtures at a total pressure of 0.12 MPa and 298 K. Three different MOFs were used: SIFSIX-1-Cu, SIFSIX-1-Cu-OMe and SIFSIX-1-Cu-$(OMe)_2$. The framework densities of

the three MOFs are, respectively, ρ = 0.867 g cm^{-3}, 0.962 g cm^{-3}, and 1.077 g cm^{-3}. The breakthrough tube has an inside diameter of 4 mm, and a packed length of 500 mm. The flow rates at the inlet, Q_0= 1 mL min^{-1}. The sample mass of the three MOFs in the packed bed were, respectively, m_{ads}, 1.2863 g, 0.8306 g, and 1.6648 g. Transient breakthrough simulations were carried out for the exact same set of operating conditions as in the experiments, using the methodology described in earlier publications [2-7]. Intra-crystalline diffusional are accounted for by taking $\frac{D_1}{r_c^2}$= 1×10^{-2} s^{-1}, $\frac{D_2}{r_c^2}$= 1×10^{-3} s^{-1} and $\frac{D_3}{r_c^2}$= 1×10^{-3} s^{-1}, where r_c is the radius of the MOF crystals packed in the tube.

Theoretical calculations

Framework atoms were considered fixed at their optimized crystallographic coordinates. All atoms were treated with Lennard-Jones (LJ) 12–6 parameters (ε and σ) [8]. The LJ parameters for all atoms were taken from the Universal Force Field (UFF) [9]. The partial charges on the framework atoms were calculated using DFT method in CP2K software. Partial atomic charges were extracted by Mulliken atom & basis function population analysis using Multiwfn 3.8 program [10].

Classical Monte Carlo (MC) simulations of C_2H_2, C_2H_4 and C_2H_6 adsorption were performed in three materials within a rigid 3 × 3 × 4 supercell of these MOF. A spherical cut-off distance corresponding to half the shortest supercell dimension length was used for the simulations. C_2H_2, C_2H_4 and C_2H_6 were modeled using polarizable potentials of the respective adsorbates that were developed previously [11]. The total potential energy of the MOF–adsorbate system was calculated through the sum of the repulsion/dispersion, stationary electrostatic, and many-body polarization energies. These were calculated using the Lennard-Jones 12–6 potential [12], partial charges with Ewald summation [13, 14], and a Thole-Applequist type model [15-18], respectively. All MC simulations were performed using the Massively Parallel Monte Carlo (MPMC) code [19].

In order to identify the global energy minimum for C_2H_2, C_2H_4 and C_2H_6 in three materials, simulated annealing (SA) calculations [20] were performed for a single molecule of each adsorbate through a canonical Monte Carlo (*NVT*) process in the considered supercell of the MOF. SA calculations for each adsorbate utilized an initial temperature of 500 K, and this temperature was scaled by a factor of 0.99999 after every 10^3 MC steps. The simulations continued until 10^6 MC steps were reached; at this point, the temperature of the system is below 15 K and the adsorbate is already localized in its energy minimum position in the MOF.

The initial configurations were further optimized to ensure a more efficient energy landscape scanning for every MOF-C_xH_x complex, and the optimized configuration having the lowest energy was used as the global minimum for the subsequent analysis and calculation. The static binding energy (at T= 0 K) was then calculated: $\Delta E_{bind} = E_{MOF} + E_{gas} - E_{total}$, in which E_{total}, E_{MOF} and E_{gas} are the calculated total energies for the gas-trapped MOF, solo MOF and isolate gas molecule replaced in the cell with same cell dimensions as MOF, respectively. Dispersion-corrected Density Functional Theory (DFT) computations were undertaken using the CP2K software package. We treated the simulation box as a periodic structure in all directions for electrostatic calculations. The Poisson equation was addressed

using a periodic boundary condition (PBC) solver. We employed the GTH-PBE exchange-correlation functional for electronic structure computations, utilizing the DZVP-MOLOPT-SR-GTH basis set. The corresponding basis set and potential files were incorporated into the input file. To consider the van der Waals interactions, we included the DFT-D3 dispersion correction. The molecular grid cutoff energy and relative cutoff energy were set to 350 Ry and 50 Ry respectively. The self-consistent field (SCF) computations were conducted with a maximum of 25 SCF iterations and a convergence threshold of 5.0E-06 for the density matrix. We utilized the Orbital Transformation (OT) method with a DIIS minimizer to facilitate convergence.

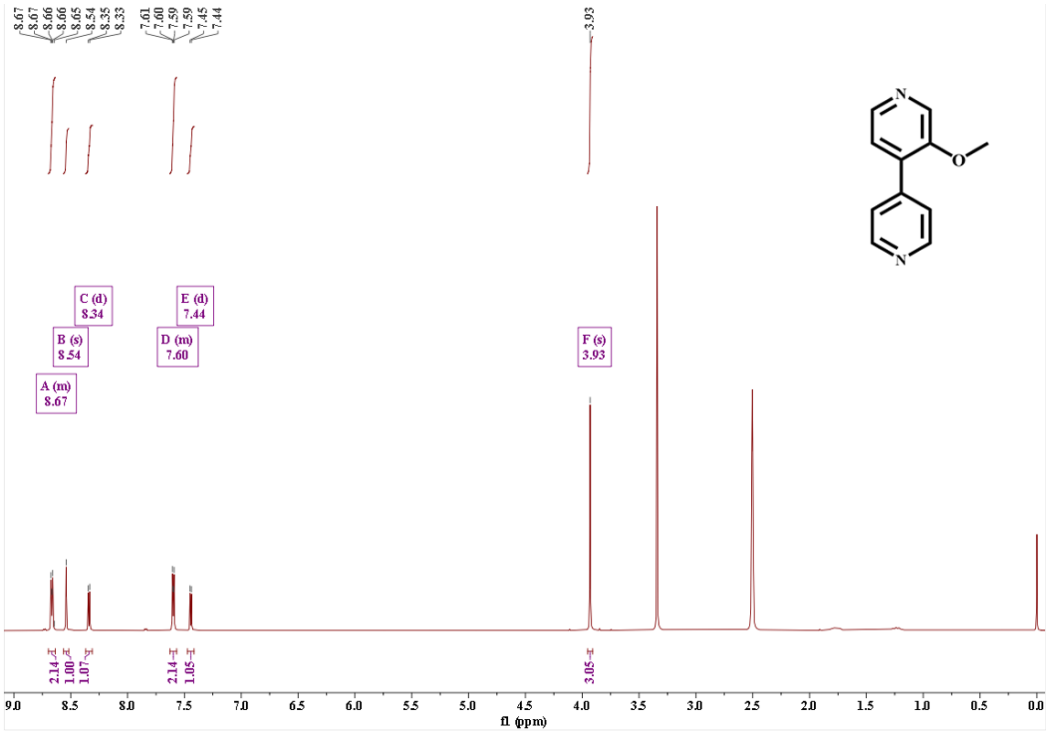

Fig. S1. The ^{1}H NMR data of ligand Bpy-OMe.

Fig. S2. The ^{1}H NMR data of ligand Bpy-(OMe)$_2$.

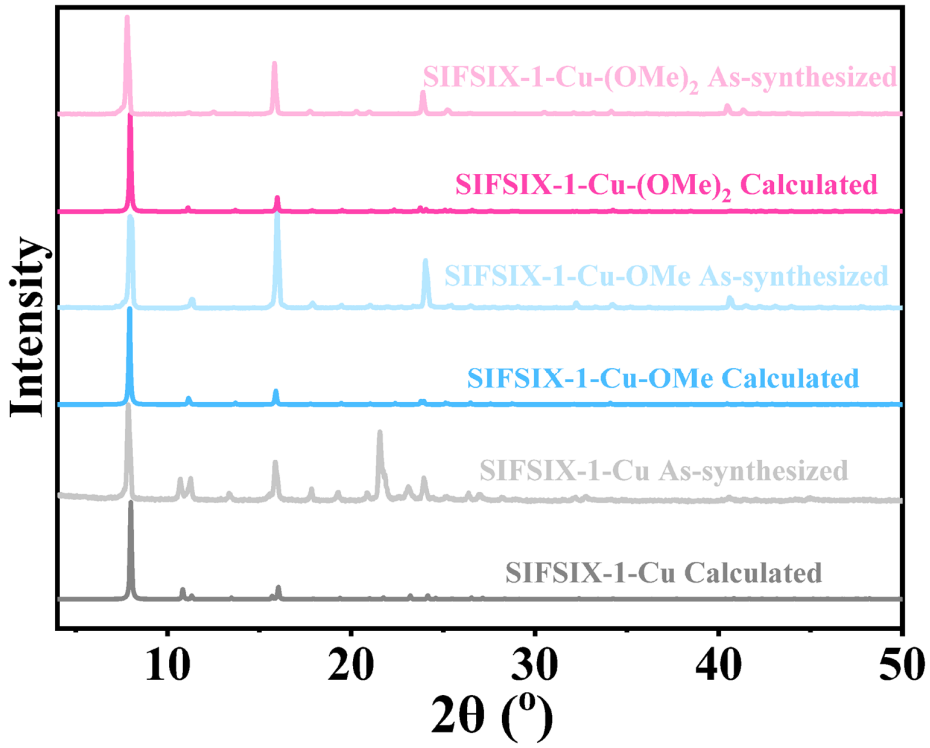

Fig. S3. The PXRD patterns of SIFSIX-1-Cu, SIFSIX-1-Cu-OMe and SIFSIX-1-Cu-$(OMe)_2$.

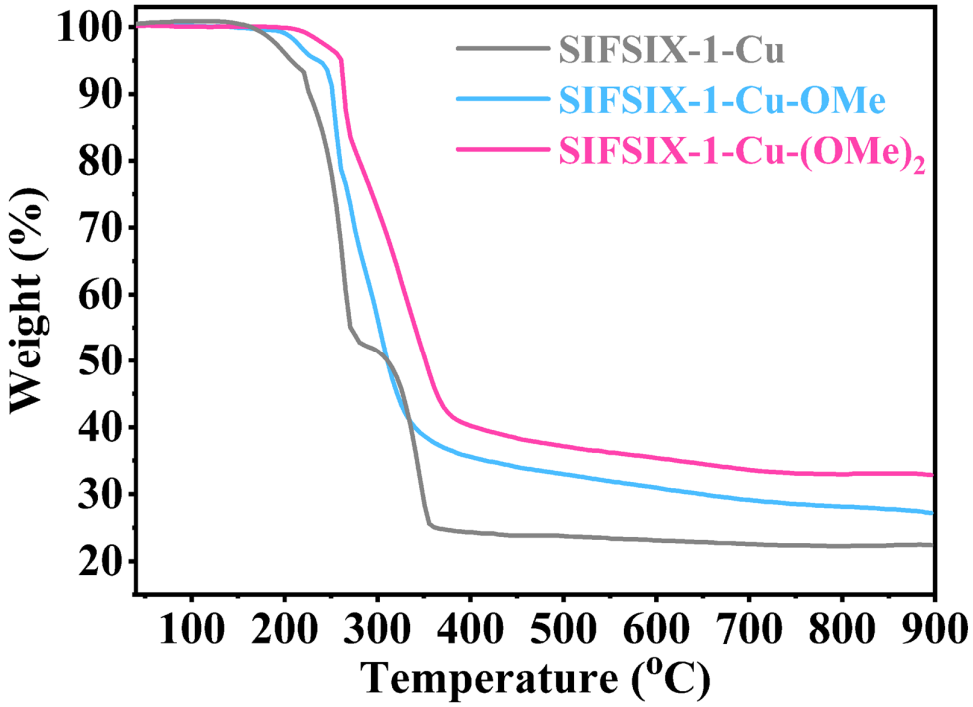

Fig. S4. The TGA curves of SIFSIX-1-Cu, SIFSIX-1-Cu-OMe and SIFSIX-1-Cu-$(OMe)_2$.

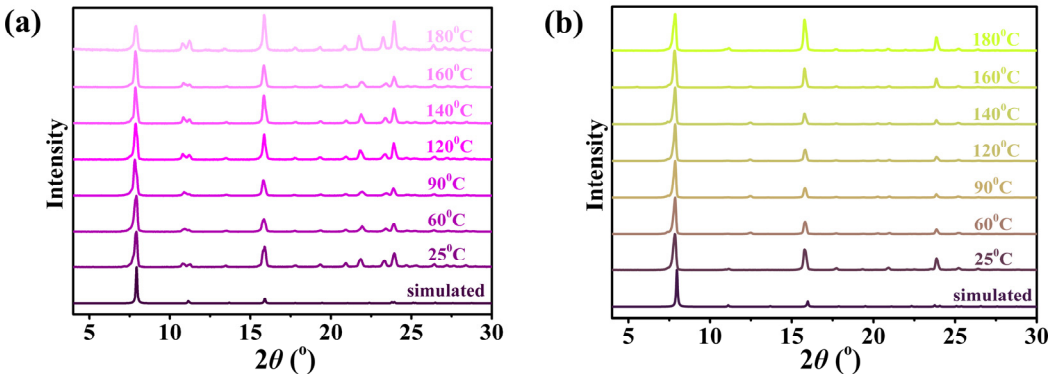

Fig. S5. The VT-PXRD patterns of (a) SIFSIX-1-Cu-OMe and (b) SIFSIX-1-Cu-$(OMe)_2$.

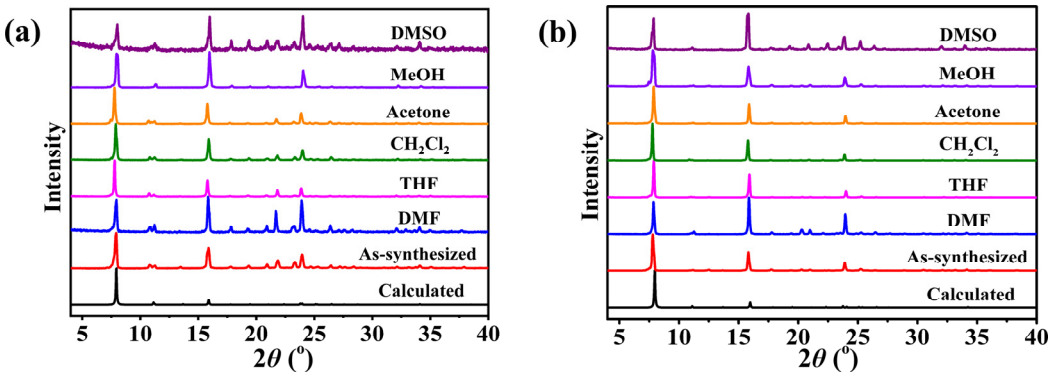

Fig. S6. The PXRD patterns after soaked in different polarity organic solvents for 24 hours of (a) SIFSIX-1-Cu-OMe and (b) SIFSIX-1-Cu-$(OMe)_2$.

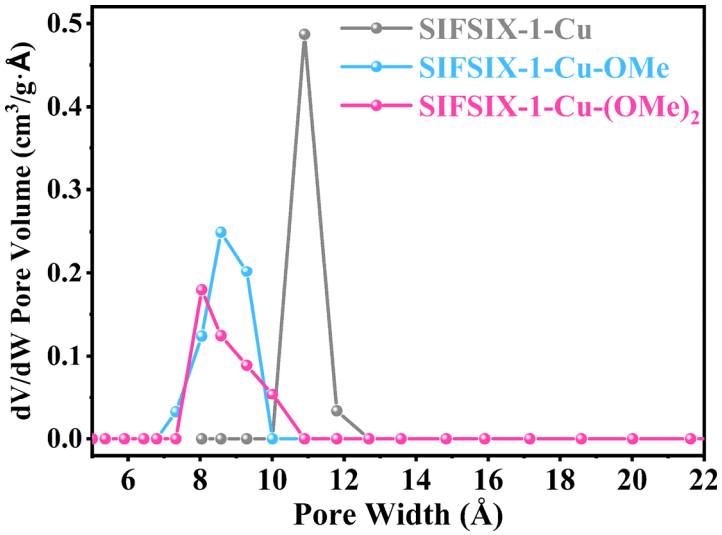

Fig. S7. The pore size distribution of SIFSIX-1-Cu, SIFSIX-1-Cu-OMe and SIFSIX-1-Cu-$(OMe)_2$ calculated by density functional theory (DFT).

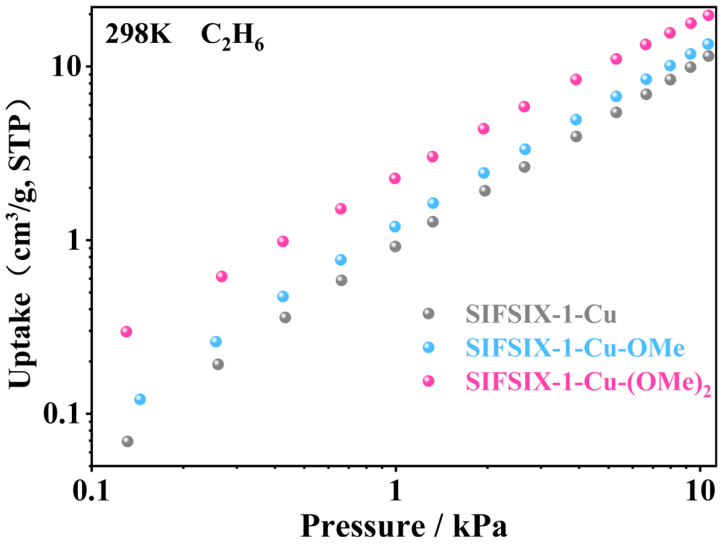

Fig. S8. C_2H_6 adsorption isotherms of SIFSIX-1-Cu, SIFSIX-1-Cu-OMe and SIFSIX-1-Cu-$(OMe)_2$ at low pressure.

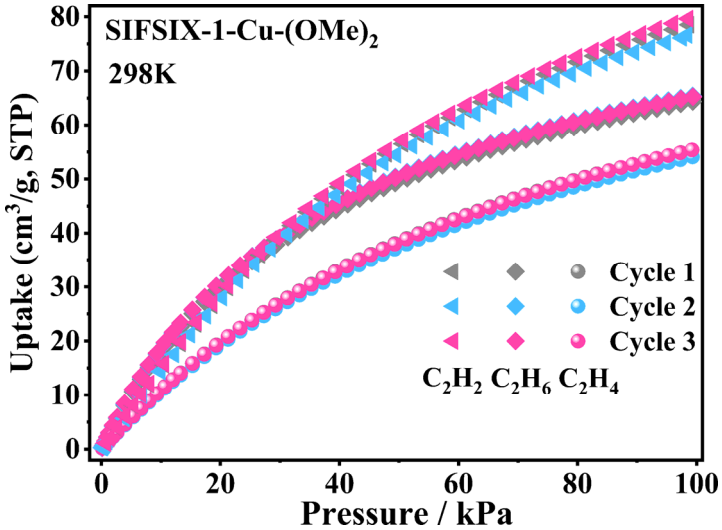

Fig. S9. C_2H_2, C_2H_6 and C_2H_4 cycles adsorption isotherms on SIFSIX-1-Cu-$(OMe)_2$ at 298 K.

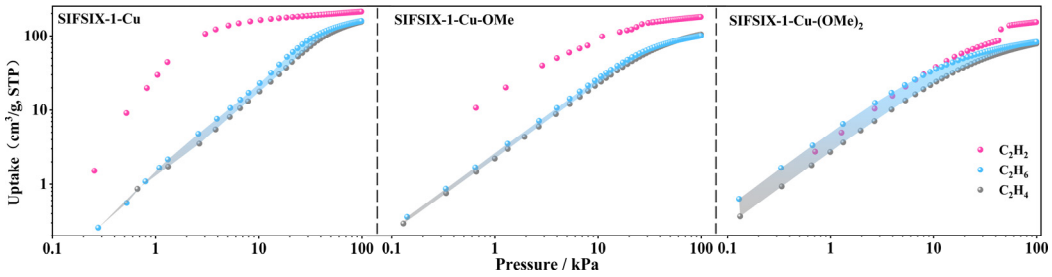

Fig. S10. C_2H_2, C_2H_4 and C_2H_6 adsorption isotherms of SIFSIX-1-Cu, SIFSIX-1-Cu-OMe and SIFSIX-1-Cu-$(OMe)_2$ at 273 K.

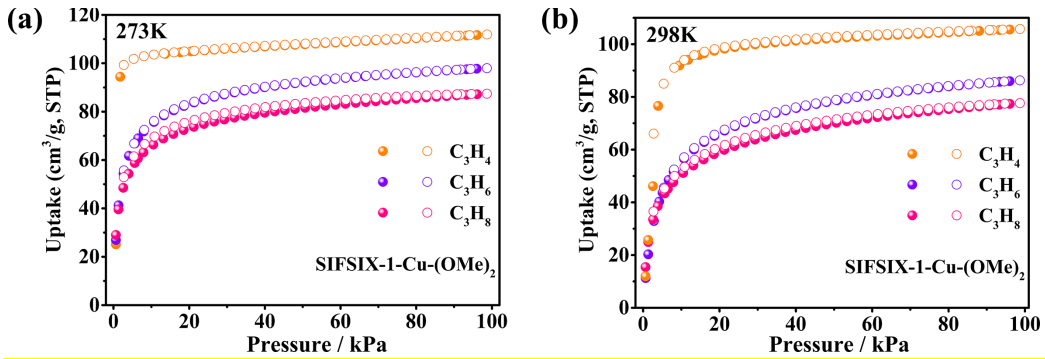

Fig. S11. The C_3-hydrocarbons adsorption isotherms on SIFSIX-1-Cu-$(OMe)_2$ at 273 K and 298 K.

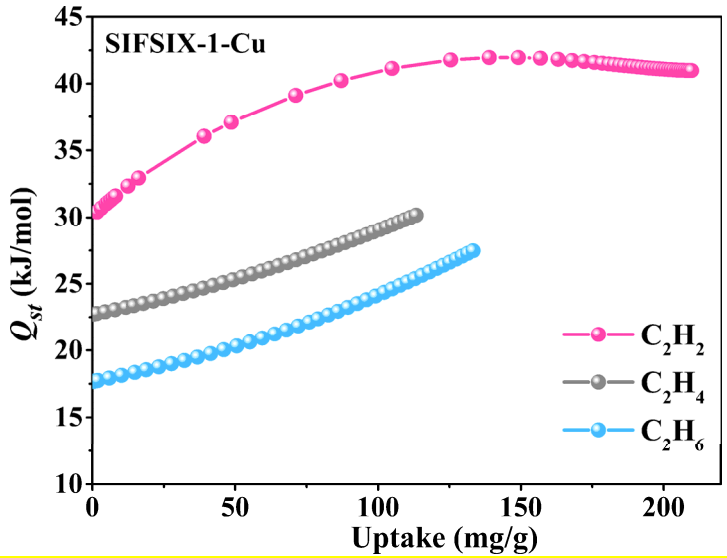

Fig. S12. Isosteric heat of adsorption (Q_{st}) of C_2H_2, C_2H_4, and C_2H_6 on SIFSIX-1-Cu.

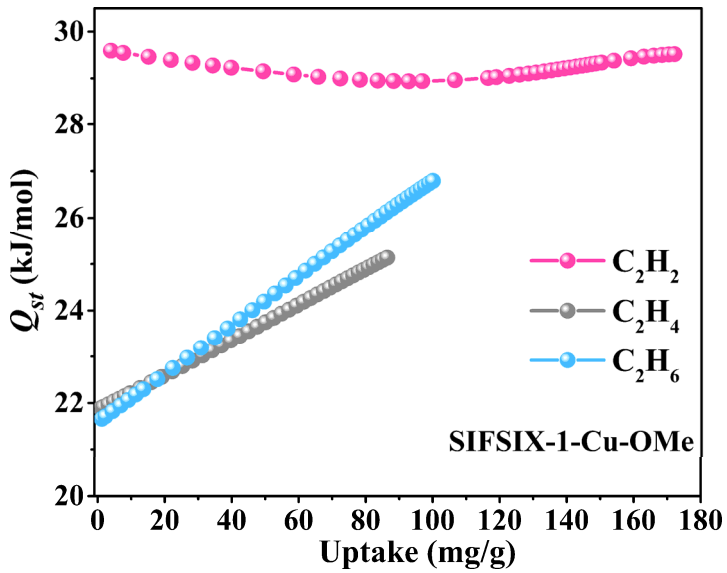

Fig. S13. Isosteric heat of adsorption (Q_{st}) of C_2H_2, C_2H_4, and C_2H_6 on SIFSIX-1-Cu-OMe.

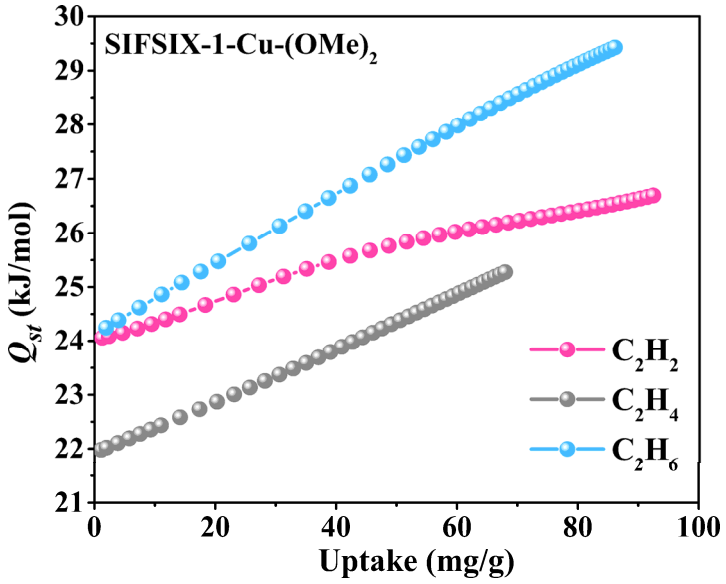

Fig. S14. Isosteric heat of adsorption (Q_{st}) of C_2H_2, C_2H_4, and C_2H_6 on SIFSIX-1-Cu-(OMe)$_2$.

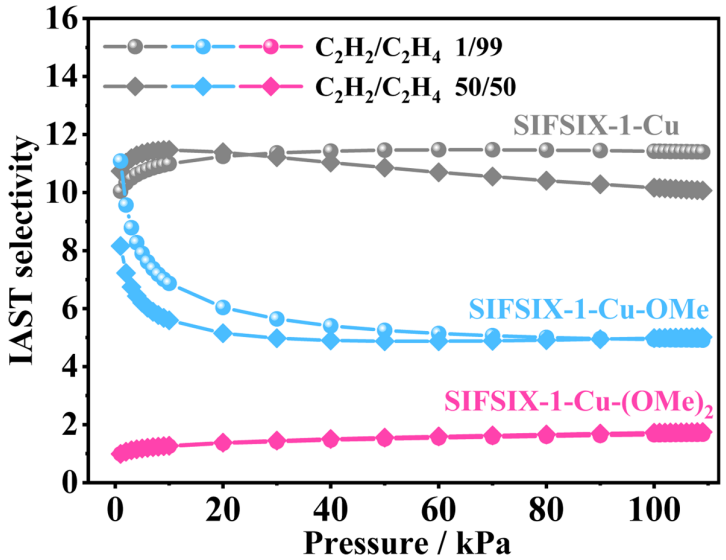

Fig. S15. The IAST selectivity of C_2H_2/C_2H_4 at 298 K for SIFSIX-1-Cu, SIFSIX-1-Cu-OMe and SIFSIX-1-Cu-(OMe)$_2$.

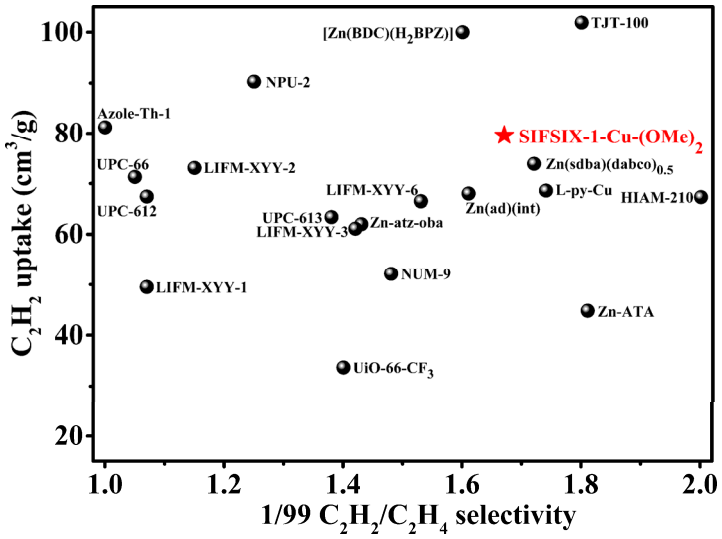

Fig. S16. Comparison of C_2H_2 uptake and 1/99 C_2H_2/C_2H_4 selectivity at 298 K and 1 bar between SIFSIX-1-Cu-$(OMe)_2$ and the reported MOFs that can realize one-step C_2H_4 purification from ternary C_2-gases mixture.

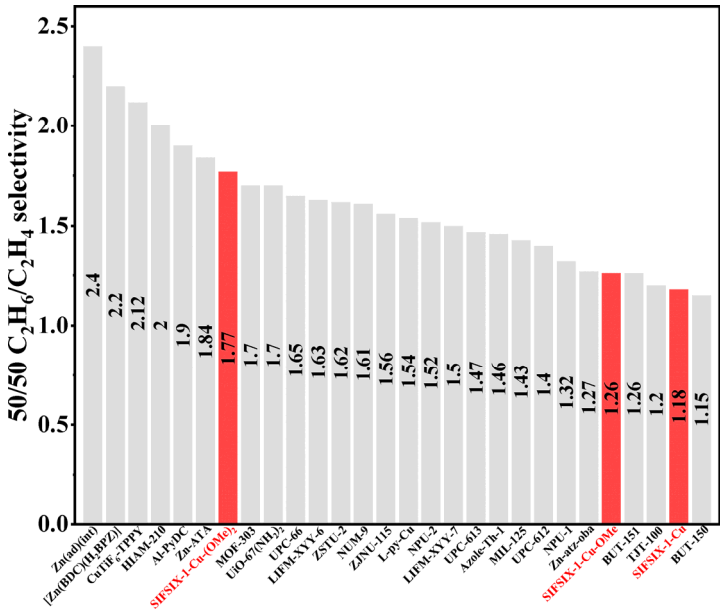

Fig. S17. Comparison of 50/50 C_2H_6/C_2H_4 selectivity at 298 K and 1 bar between three materials and the reported MOFs that can realize one-step C_2H_4 purification from ternary C_2-gases mixture.

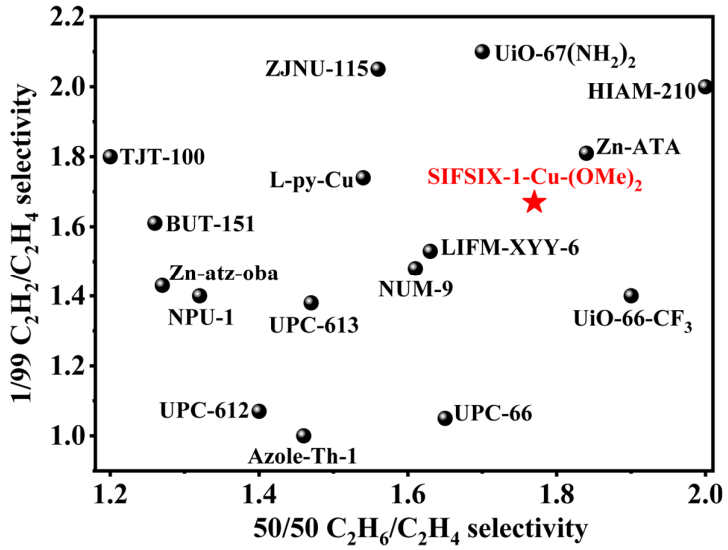

Fig. S18. Comparison of 50/50 C_2H_6/C_2H_4 selectivity and 1/99 C_2H_2/C_2H_4 selectivity at 298 K and 1 bar between SIFSIX-1-Cu-$(OMe)_2$ and the reported MOFs that can realize one-step C_2H_4 purification from ternary C_2-gases mixture.

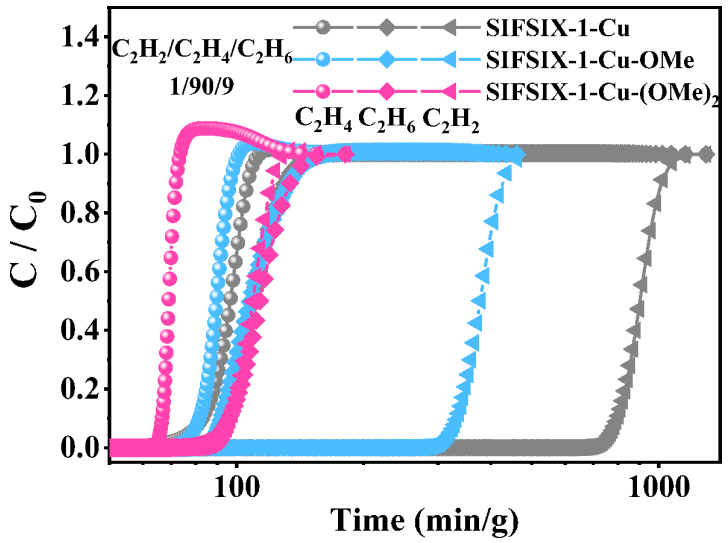

Fig. S19. The simulated breakthrough curves of 1/90/9 $C_2H_2/C_2H_4/C_2H_6$ in SIFSIX-1-Cu, SIFSIX-1-Cu-OMe and SIFSIX-1-Cu-$(OMe)_2$ at 298 K.

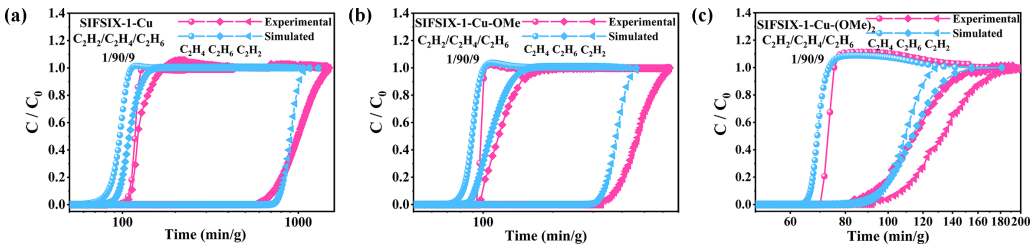

Fig. S20. The simulated and experimental breakthrough curves of 1/90/9 $C_2H_2/C_2H_4/C_2H_6$ at 298 K in (a) SIFSIX-1-Cu; (b) SIFSIX-1-Cu-OMe; (c) SIFSIX-1-Cu-$(OMe)_2$.

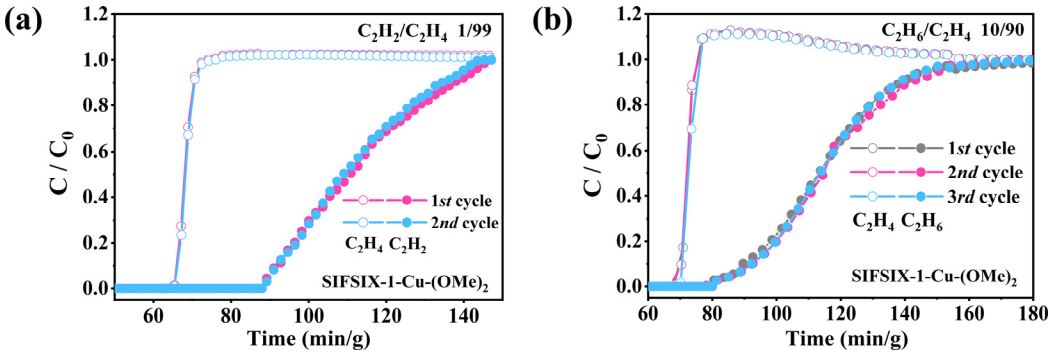

Fig. S21. Cycles breakthrough experiments of SIFSIX-1-Cu-(OMe)2 at 298 K for (a) 1/99 C_2H_2/C_2H_4; (b) 10/90 C_2H_6/C_2H_4.

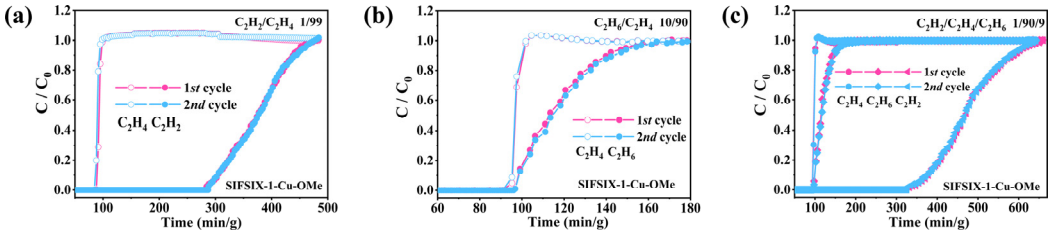

Fig. S22. Cycles breakthrough experiments of SIFSIX-1-Cu-OMe at 298 K for (a) 1/99 C_2H_2/C_2H_4; (b) 10/90 C_2H_6/C_2H_4;. (c) 1/90/9 $C_2H_2/C_2H_4/C_2H_6$.

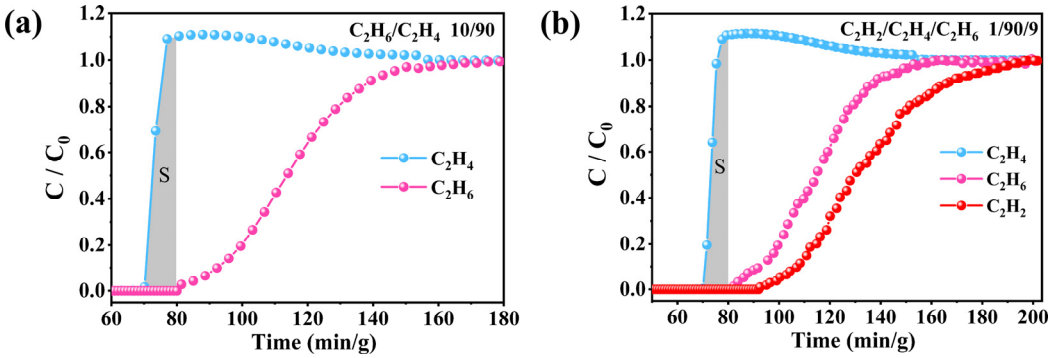

Fig. S23. Calculation the C_2H_4 productivity in binary mixture and ternary mixture breakthrough experiments:

$$Q_{C_2H_4} = \nu \times V\,\% \times S$$

$Q_{C_2H_4}$ is the C_2H_4 productivity (L/kg), ν is the flow rate of gas mixture (mL/min), V % is the molar fraction of C_2H_4 in gas mixture.

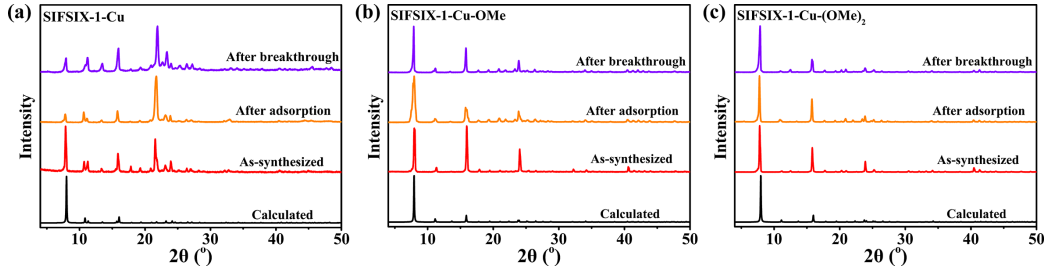

Fig. S24. The PXRD patterns of SIFSIX-1-Cu (a), SIFSIX-1-Cu-OMe (b) and SIFSIX-1-Cu-(OMe)2 (c) after adsorption and breakthrough experiments.

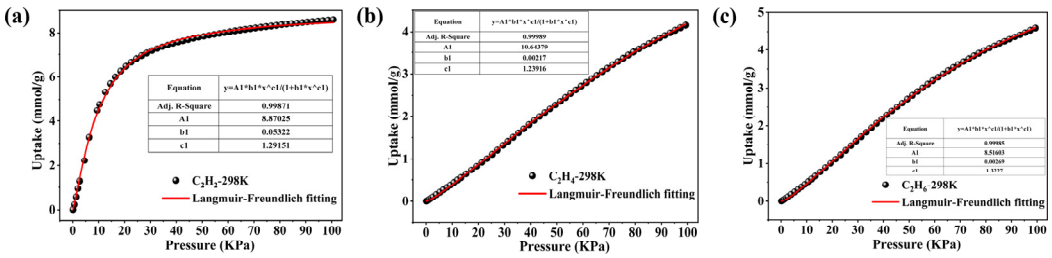

Fig. S25. (a) C_2H_2, (b) C_2H_4 and (c) C_2H_6 adsorption isotherms at 298 K in SIFSIX-1-Cu with single-site Langmuir-Freundlich model fits.

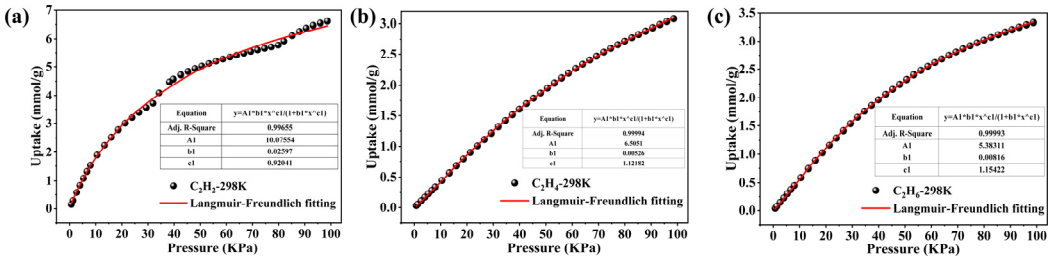

Fig. S26. (a) C_2H_2, (b) C_2H_4 and (c) C_2H_6 adsorption isotherms at 298 K in SIFSIX-1-Cu-OMe with single-site Langmuir-Freundlich model fits.

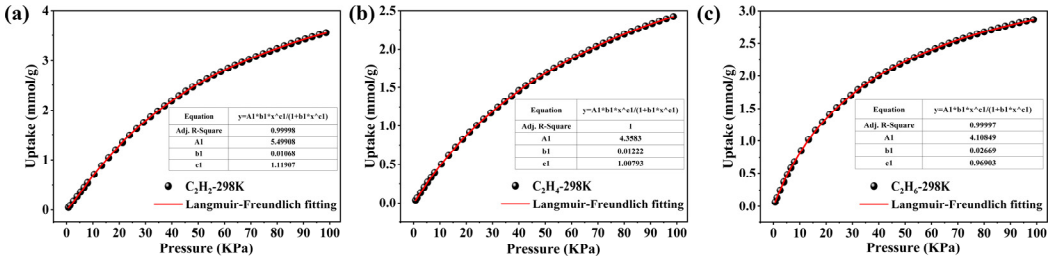

Fig. S27. (a) C_2H_2, (b) C_2H_4 and (c) C_2H_6 adsorption isotherms at 298 K in SIFSIX-1-Cu-$(OMe)_2$ with single-site Langmuir-Freundlich model fits.

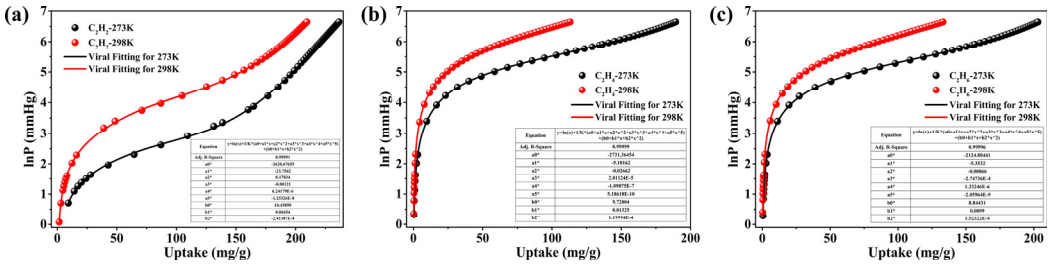

Fig. S28. (a) C_2H_2, (b) C_2H_4 and (c) C_2H_6 adsorption isotherms in SIFSIX-1-Cu with virial fitting.

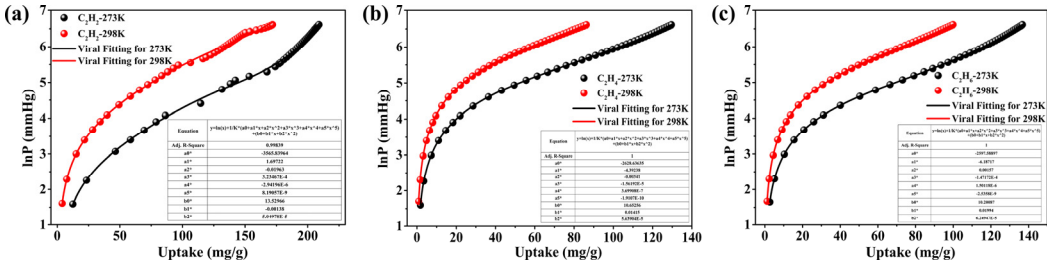

Fig. S29. (a) C_2H_2, (b) C_2H_4 and (c) C_2H_6 adsorption isotherms in SIFSIX-1-Cu-OMe with virial fitting.

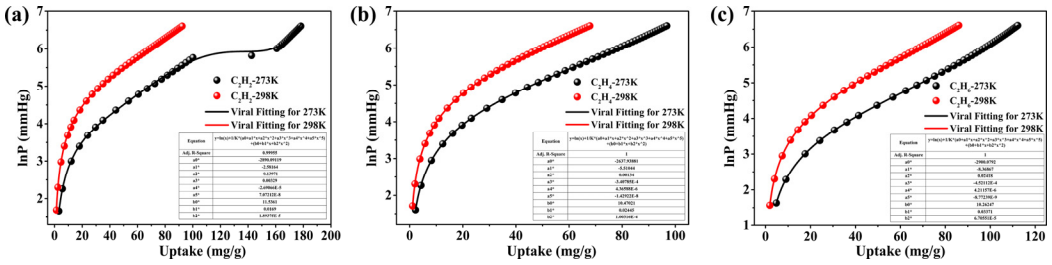

Fig. S30. (a) C_2H_2, (b) C_2H_4 and (c) C_2H_6 adsorption isotherms in SIFSIX-1-Cu-$(OMe)_2$ with virial fitting.

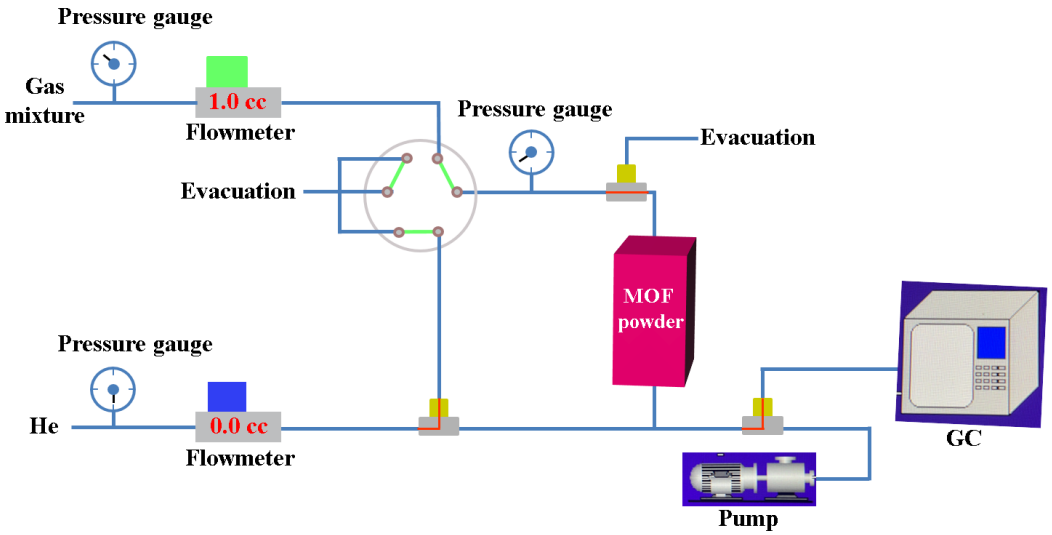

Fig. S31. Schematic diagram of breakthrough system.

Table S1. Physical and chemical properties of C_2H_2, C_2H_4 and C_2H_6.

Molecular	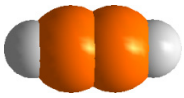	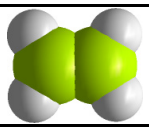	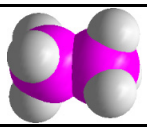
Molecular dimensions ($Å^3$)	3.32×3.34×5.70	3.28 × 4.18 × 4.84	3.81 ×4.08 × 4.82
Kinetic diameter (Å)	3.3	4.2	4.4
Quadrupole moment ($\times 10^{-26}$ esu cm^2)	7.2	1.5	0.65
Polarizability ($\times 10^{-25}$ cm^3)	33.3-39.3	42.5	44.3-44.7
Boiling point (K)	188.4	169.4	184.5

Table S2. Crystal data and structure refinement.

Complex	SIFSIX-1-Cu	SIFSIX-1-Cu-OMe	SIFSIX-1-Cu-$(OMe)_2$
Empirical formula	$C_{20}H_{16}CuF_6N_4Si$	$C_{22}H_{14}CuF_6N_4O_2Si$	$C_{24}H_{20}CuF_6N_4O_4Si$
Formula weight	518.00	572.00	634.07
Temperature	100 K	100 K	100 K
Crystal system	tetragonal	tetragonal	tetragonal
Space group	*P4/mmm*	*P4/mmm*	*P4/mmm*
a/Å	11.08829(18)	11.0899(2)	11.0854(2)
b/Å	11.08829(18)	11.0899(2)	11.0854(2)
c/Å	8.0677(2)	8.0251(3)	7.9538(2)
α/°	90	90	90
β/°	90	90	90
γ/°	90	90	90
Volume/$Å^3$	991.93(4)	986.97(5)	977.41(4)
Z	1	1	1
ρ_{calc}g/cm^3	0.867	0.962	1.077
μ/mm^{-1}	1.404	1.491	1.587
F(000)	261.0	287.0	321.0
Goodness-of-fit on F^2	1.184	0.891	1.214
Final R indexes [I>=2σ(I)]	R_1 = 0.0666, wR_2 = 0.1753	R_1 = 0.1055, wR_2 = 0.3507	R_1 = 0.0923, wR_2 = 0.3000
Final R indexes [all data]	R_1 = 0.0712, wR_2 = 0.1776	R_1 = 0.1090, wR_2 = 0.3545	R_1 = 0.0940, wR_2 = 0.3021
CCDC Number	142080	**2351841**	**2351842**

Table S3. Comparison of adsorption capacity, IAST selectivity, and initial Q_{st} of some famous C_2H_2/C_2H_6-selective MOFs.

MOFs	Adsorption capacity (cm^3/g)			IAST selectivity			Q_{st} at zero coverage (kJ/mol)			Ref
	C_2H_2 (1 bar)	C_2H_6 (0.1 / 1 bar)	C_2H_4 (1 bar)	C_2H_2/C_2H_4 (1/99)	C_2H_6/C_2H_4 (50/50)	C_2H_6/C_2H_4 (10/90)	C_2H_2	C_2H_4	C_2H_6	
SIFSIX-1-Cu-(OMe)$_2$	**79.6**	**19.7 / 65.2**	**55.3**	**1.67**	**1.77**	**1.79**	**24.1**	**22.0**	**24.2**	**This work**
SIFSIX-1-Cu-OMe	**148.2**	**13.5 / 75.4**	**70.1**	**4.91**	**1.26**	**1.27**	**29.6**	**21.9**	**21.7**	**This work**
SIFSIX-1-Cu	**192.7**	**11.5 / 102.9**	**93.1**	**11.40**	**1.18**	**1.18**	**30.4**	**22.7**	**17.7**	**This work**
TJT-100	101.9	27.1 / 82.9	76.9	1.80	1.20[b]	-	31	25	29	[21]
Azole-Th-1	81.2	19.0 / 100.1	81.1	1.00	1.46	1.44	25.4	26.1	28.6	[22]
UiO-67-(NH$_2$)$_2$	132.2	23.3 / 119.2	96.8	2.10	1.70	-	27.4	24.5	26.5	[23]

UiO-67	46.8	5.2 / 68.3	47.7	1.07	1.49	-	23.3	23.2	24.7	[23]
UPC-612	67.4	10.1 / 80.2	65.3	1.07[a]	1.40	1.40	23.9	16.9	22.4	[24]
UPC-613	63.4	15.7 / 57.1	51.7	1.38[a]	1.47	1.47	30.4	28.5	31.8	[24]
MOF-525	59.4	6.9 / 59.4	47.3	1.44[a]	1.25	1.25	15.8	16.7	19.9	[24]
MOF-525(Co)	58.7	7.8 / 49.7	43.0	1.95[a]	1.10	1.10	18.6	23.4	20.7	[24]
ZJNU-115	106.0	24.0 / 94.2	84.0	2.05	1.56	-	29.2	27.7	28.2	[25]
NUM-9	52.1	24.0 / 55.6	49.9	1.48	1.61	1.62	35.8	32.3	35.8	[26]
NPU-1	114.0	25.1 / 100.8	94.1	1.40[a]	1.32	-	27.9	23.9	29.1	[27]
NPU-2	90.3	13.0 / 99.0	77.3	1.25[a]	1.52	-	21.0	18.2	19.6	[27]
NPU-3	57.8	7.2 / 75.3	49.7	1.32[a]	3.21	-	19.9	17.8	18.7	[27]
Zn(ad)(int)	68.0	41.0 / 51.9	49.4	1.61	2.40	2.40	34.7	28.9	33.2	[28]

Zn-ATA	44.8	18.0 / 24.1	26.8	1.81	-	1.84	24.5	27.4	32.5	[29]
[Zn(BDC)(H_2BPZ)]	100.0	44.0 / 81.4	73.6	1.60[a]	-	2.20	28.7	23.2	31.8	[30]
$CuTiF_6$-TPPY	81.1	29.8 / 63.2	54.2	5.03	2.12	2.12	36.5	29.6	34.2	[31]
UiO-66-CF_3	33.7	10.2 / 30.9	25.4	1.40[a]	1.90	1.90	24.3	22.2	24.3	[32]
HIAM-210	67.3	19.0 / 52.4	47.4	2.00[a]	2.00	-	34.3	22.7	31.2	[33]
L-py-Cu	68.6	20.0 / 48.5	48.4	1.74[a]	1.54	-	34.4	25.6	29.2	[34]
Ni(sdba)$(dabco)_{0.5}$	98.8	38.1 / 70.6	67.0	2.28[a]	2.47	2.57	32.8	28.2	29.8	[35]
Zn(sdba)$(dabco)_{0.5}$	73.9	27.8 / 63.4	60.0	1.72[a]	2.05	-	32.4	27.9	29.0	[35]
MOF-303	177.9	35.8 / 112.0	-	2.40	1.70	-	31.7	24.3	25.1	[36]
ZJNU-7	112.8	31.8 / 92.5	85.2	1.77	1.56	1.58	34.1	29.3	29.7	[37]
Zn-atz-oba	62.0	14.3 / 45.7	45.2	1.43[a]	1.27	-	27.5	27	30	[38]

UPC-66	71.3	17.2 / 61.9	54.0	1.05[a]	1.65	-	17.6	17.8	15.6	[39]
BUT-150	123.9	29.8 / 96.3	95.4	1.82[a]	1.15	-	30.5	23.7	23.9	[40]
BUT-151	107.5	23.7 / 89.4	83.3	1.61[a]	1.26	-	36.8	23.9	31.1	[40]
Al-MOFM$_{15}$	63.8	13.9 / 49.9	28.9	3.32[a]	2.51	-	40.2	32.8	45	[41]
MIL-125	157.9	17.0 / 108.2	89.1	2.32	1.43	-	17.6	17	23.6	[42]
NH_2-MIL-125	175.2	20.4 / 105.1	98.8	3.75	1.18	-	-	-	-	[42]
MUV-11	89.2	13.2 / 41.0	38.5	6.92	1.53	-	-	-	-	[42]
ZSTU-2	69.7	20.6 / 61.2	52.6	2.36	1.62	-	-	-	-	[42]
Al-PyDC	184.6	- / 94.1	77.1	4.30	1.90	-	35.3	27.8	30.1	[43]
LIFM-28	19.5	4.0 / 21.8	17.4	1.04	1.24	-	26.6	26.0	28.8	[44]
PCN-700	21.0	4.0 / 28.6	19.4	1.07	1.53	-	25.6	23.6	26.3	[44]

LIFM-XYY-1	49.5	11.0 / 60.4	46.7	1.07	1.51	-	29.6	28.8	29.5	[44]
LIFM-XYY-2	73.1	15.0 / 81.8	65.3	1.15	1.48	-	33.1	28.8	29.5	[44]
LIFM-XYY-3	61.1	9.0 / 56.7	47.0	1.42	1.33	-	31.0	28.5	29.6	[44]
LIFM-XYY-4	79.3	15.0 / 87.1	61.3	1.41	1.68	-	27.2	25.0	29.3	[44]
LIFM-XYY-5	68.8	12.0 / 75.9	57.4	1.31	1.53	-	25.9	18.3	26.7	[44]
LIFM-XYY-6	66.5	12.0 / 66.9	50.1	1.53	1.63	-	37.1	31.5	32.2	[44]
LIFM-XYY-7	108.9	18.0 / 117.2	91.2	1.24	1.50	-	22.3	23.0	24.9	[44]
LIFM-XYY-8	85.3	15.0 / 94.3	73.9	1.14	1.47	-	25.9	26.7	27.4	[44]

[a] IAST selectivity for 50/50 C_2H_2/C_2H_4.

[b] IAST selectivity for 1/99 C_2H_6/C_2H_4.

Table S4. The detailed binding energies for the E_{total}, E_{MOF} and E_{gas} of SIFSIX-1-Cu, SIFSIX-1-Cu-OMe and SIFSIX-1-Cu-$(OMe)_2$.

MOFs	Gas Molecules	E_{total} (Ha)	E_{MOF} (Ha)	E_{gas} (Ha)	ΔE_{bind} (Ha)	**ΔE_{bind} (kJ/mol)**
SIFSIX-1-Cu	C_2H_2	-733.1679	-720.7042	-12.4370	-0.0267	**-69.9779**
	C_2H_4	-734.4052	-720.7043	-13.6813	-0.0196	**-51.3559**
	C_2H_6	-735.6244	-720.7046	-14.9062	-0.0136	**-35.7150**
SIFSIX-1-Cu-OMe	C_2H_2	-824.5969	-812.1367	-12.4370	-0.0232	**-61.0181**
	C_2H_4	-825.8368	-812.1367	-13.6813	-0.0188	**-49.2818**
	C_2H_6	-827.0614	-812.1378	-14.9062	-0.0174	**-45.5602**
SIFSIX-1-Cu-$(OMe)_2$	C_2H_2	-916.0243	-903.5706	-12.4372	-0.0165	**-43.2693**
	C_2H_4	-917.2662	-903.5691	-13.6813	-0.0159	**-41.6176**
	C_2H_6	-918.4933	-903.5697	-14.9063	-0.0173	**-45.5220**

Table S5. The charge values and Lennard-Jones (LJ) potentials for C_2H_2, C_2H_4, and C_2H_6 molecules.

Gas molecules	Atom	Partial charge on atom (in e)	Lennard-Jones ε (K)	Lennard-Jones σ (Å)
C_2H_2	C	-0.29121	81.35021	3.40149
	H	0.29121	0.00026	4.77683
C_2H_4	C	-0.34772	69.08116	3.51622
	H	0.17386	3.169	2.41504
C_2H_6	C	-0.04722	141.80885	3.28897
	H	0.01574	0.62069	2.88406

References

[1] T. Ohmura, Y. Morimasa, M. Suginome, Organocatalytic diboration involving "reductive addition" of a boron-boron σ-bond to 4,4′-bipyridine, J. Am. Chem. Soc. 137 (2015) 2852-2855.

[2] R. Krishna, The maxwell-stefan description of mixture diffusion in nanoporous crystalline materials, Microporous Mesoporous Mater. 185 (2014) 30-50.

[3] R. Krishna, Methodologies for evaluation of metal-organic frameworks in separation applications, RSC Adv. 5 (2015) 52269-52295.

[4] R. Krishna, Screening metal-organic frameworks for mixture separations in fixed-bed adsorbers using a combined selectivity/capacity metric, RSC Adv. 7 (2017) 35724-35737.

[5] R. Krishna, Methodologies for screening and selection of crystalline microporous materials in mixture separations, Sep. Purif. Technol. 194 (2018) 281-300.

[6] R. Krishna, Metrics for evaluation and screening of metal-organic frameworks for applications in mixture separations, Acs Omega 5 (2020) 16987-17004.

[7] R. Krishna, Synergistic and antisynergistic intracrystalline diffusional influences on mixture separations in fixed-bed adsorbers, Precis. Chem. 1 (2023) 83-93.

[8] J. E. Jones, On the determination of molecular fields. - II. From the equation of state of a gas, Proc. R. Soc. A 106 (1924) 463-477.

[9] A. K. Rappe, C. J. Casewit, K. S. Colwell, W. A. Goddard, W. M. Skiff, UFF, a full periodic-table force-field for molecular mechanics and molecular-dynamics simulations, J. Am. Chem. Soc. 114 (1992) 10024-10035.

[10] T. Lu, F. Chen, Multiwfn: A multifunctional wavefunction analyzer, J. Comput. Chem. 33 (2012) 580-592.

[11] D. M. Franz, Z. E. Dyott, K. A. Forrest, A. Hogan, P. Tony, B. Space, Simulations of hydrogen, carbon dioxide, and small hydrocarbon sorption in a nitrogen-rich *rht*-metal-organic framework, Phys. Chem. Chem. Phys. 20 (2018) 1761-1777.

[12] K.-J. Chen, H. S. Scott, D. G. Madden, T. Pham, A. Kumar, A. Bajpai, M. Lusi, K. A. Forrest, B. Space, J. J. Perry, M. J. Zaworotko, Benchmark C_2H_2/CO_2 and CO_2/C_2H_2 separation by two closely related hybrid ultramicroporous materials, Chem 1 (2016) 753-765.

[13] P. P. Ewald, Die berechnung optischer und elektrostatischer gitterpotentiale, Ann. Phys. 64 (2006) 253-287.

[14] B. A. Wells, A. L. Chaffee, Ewald summation for molecular simulations, J. Chem. Theory. 11 (2015) 3684-3695.

[15] J. Applequist, J. R. Carl, K. K. Fung, Atom dipole interaction model for molecular polarizability-application to polyatomic-molecules and determination of atom polarizabilities, J. Am. Chem. Soc. 94 (1972) 2952-2960.

[16] B. T. Thole, Molecular polarizabilities calculated with a modified dipole interaction, Chem. Phys. 59 (1981) 341-350.

[17] K. A. Bode, J. Applequist, A new optimization of atom polarizabilities in halomethanes, aldehydes, ketones, and amides by way of the atom dipole interaction model, J. Phys. Chem. 100 (1996) 17820-17824.

[18] K. McLaughlin, C. R. Cioce, T. Pham, J. L. Belof, B. Space, Efficient calculation of many-body induced electrostatics in molecular systems, J. Chem. Phys. 139 (2013) 184112.

[19] D. M. Franz, J. L. Belof, K. McLaughlin, C. R. Cioce, B. Tudor, A. Hogan, L. Laratelli, M. Mulcair, M. Mostrom, A. Navas, A. C. Stern, K. A. Forrest, T. Pham, B. Space, MPMC and MCMD: Free high-performance simulation software for atomistic systems, Adv. Theory Simul. 2 (2019) 1900113.

[20] S. Kirkpatrick, C. D. Gelatt, M. P. Vecchi, Optimization by simulated annealing, Science 220 (1983) 671-680.

[21] H.-G. Hao, Y.-F. Zhao, D.-M. Chen, J.-M. Yu, K. Tan, S. Ma, Y. Chabal, Z.-M. Zhang, J.-M. Dou, Z.-H. Xiao, G. Day, H.-C. Zhou, T.-B. Lu, Simultaneous trapping of C_2H_2 and C_2H_6 from a ternary mixture of $C_2H_2/C_2H_4/C_2H_6$ in a robust metal-organic framework for the purification of C_2H_4, Angew. Chem. Int. Ed. 57 (2018) 16067-16071.

[22] Z. Xu, X. Xiong, J. Xiong, R. Krishna, L. Li, Y. Fan, F. Luo, B. Chen, A robust Th-azole framework for highly efficient purification of C_2H_4 from a $C_2H_4/C_2H_2/C_2H_6$ mixture, Nat. Commun. 11 (2020) 3163.

[23] X. W. Gu, J. X. Wang, E. Wu, H. Wu, W. Zhou, G. Qian, B. Chen, B. Li, Immobilization of lewis basic sites into a stable ethane-selective MOF enabling one-step separation of ethylene from a ternary mixture, J. Am. Chem. Soc. 144 (2022) 2614-2623.

[24] Y. Wang, C. Hao, W. Fan, M. Fu, X. Wang, Z. Wang, L. Zhu, Y. Li, X. Lu, F. Dai, Z. Kang, R. Wang, W. Guo, S. Hu, D. Sun, One-step ethylene purification from an acetylene/ethylene/ethane ternary mixture by cyclopentadiene cobalt-functionalized metal-organic frameworks, Angew. Chem. Int. Ed. 60 (2021) 11350-11358.

[25] L. Fan, P. Zhou, X. Wang, L. Yue, L. Li, Y. He, Rational construction and performance regulation of an In(III)-tetraisophthalate framework for one-step adsorption-phase purification of C_2H_4 from C_2 hydrocarbons, Inorg. Chem. 60 (2021) 10819-10829.

[26] S.-Q. Yang, F.-Z. Sun, P. Liu, L. Li, R. Krishna, Y.-H. Zhang, Q. Li, L. Zhou, T.-L. Hu, Efficient purification of ethylene from C_2 hydrocarbons with an C_2H_6/C_2H_2-selective metal-organic framework, ACS Appl. Mater. Interfaces 13 (2021) 962-969.

[27] B. Zhu, J.-W. Cao, S. Mukherjee, T. Pham, T. Zhang, T. Wang, X. Jiang, K. A. Forrest, M. J.

Zaworotko, K.-J. Chen, Pore engineering for one-step ethylene purification from a three-component hydrocarbon mixture, J. Am. Chem. Soc. 143 (2021) 1485-1492.

[28] Q. Ding, Z. Zhang, Y. Liu, C. Kungang, R. Krishna, S. Zhang, One-step ethylene purification from ternary mixtures in a metal-organic framework with customized pore chemistry and shape, Angew. Chem. Int. Ed. 61 (2022) e202208134.

[29] Q. Ding, Z. Zhang, P. Zhang, C. Yu, C.-H. He, X. Cui, H. Xing, One-step ethylene purification from ternary mixture by synergetic molecular shape and size matching in a honeycomb-like ultramicroporous material, Chem. Eng. J. 450 (2022) 138272.

[30] G.-D. Wang, Y.-Z. Li, W.-J. Shi, L. Hou, Y.-Y. Wang, Z. Zhu, One-step C_2H_4 purification from ternary $C_2H_6/C_2H_4/C_2H_2$ mixtures by a robust metal-organic framework with customized pore environment, Angew. Chem. Int. Ed. 61 (2022) e202205427.

[31] P. Zhang, Y. Zhong, Y. Zhang, Z. Zhu, Y. Liu, Y. Su, J. Chen, S. Chen, Z. Zeng, H. Xing, S. Deng, J. Wang, Synergistic binding sites in a hybrid ultramicroporous material for one-step ethylene purification from ternary C_2 hydrocarbon mixtures, Sci. Adv. 8 (2022) eabn9231.

[32] J. Liu, J. Miao, H. Wang, Y. Gai, J. Li, Enhanced one-step purification of C_2H_4 from $C_2H_2/C_2H_4/C_2H_6$ mixtures by fluorinated Zr-MOF, AlChE J. 69 (2023) e18021.

[33] J. Liu, H. Wang, J. Li, Pillar-layer Zn-triazolate-dicarboxylate frameworks with a customized pore structure for efficient ethylene purification from ethylene/ethane/acetylene ternary mixtures, Chem. Sci. 14 (2023) 5912-5917.

[34] L.-L. Ma, N. An, F.-A. Guo, H. Wang, G.-P. Yang, Y.-Y. Wang, Separation of $C_2H_2/C_2H_4/C_2H_6$ and C_2H_2/CO_2 in a nitrogen-rich copper-based microporous metal-organic framework, Inorg. Chem. 62 (2023) 13698-13701.

[35] H. Shuai, J. Liu, Y. Teng, X. Liu, L. Wang, H. Xiong, P. Wang, J. Chen, S. Chen, Z. Zhou, S. Deng, Pillar-layered metal-organic frameworks with benchmark C_2H_2/C_2H_4 and C_2H_6/C_2H_4 selectivity for one-step C_2H_4 production, Sep. Purif. Technol. 323 (2023) 124392.

[36] H.-M. Wen, C. Yu, M. Liu, C. Lin, B. Zhao, H. Wu, W. Zhou, B. Chen, J. Hu, Construction of negative electrostatic pore environments in a scalable, stable and low-cost metal-organic framework for one-step ethylene purification from ternary mixtures, Angew. Chem. Int. Ed. 62 (2023) e202309108.

[37] Z. Z. Jiang, L. H. Fan, P. Zhou, T. T. Xu, S. M. Hu, J. X. Chen, D. L. Chen, Y. B. He, An aromatic-rich cage-based MOF with inorganic chloride ions decorating the pore surface displaying the preferential adsorption of C_2H_2 and C_2H_6 over C_2H_4, Inorg. Chem. Front. 8 (2021) 1243-1252.

[38] J.-W. Cao, S. Mukherjee, T. Pham, Y. Wang, T. Wang, T. Zhang, X. Jiang, H.-J. Tang, K. A. Forrest, B. Space, M. J. Zaworotko, K.-J. Chen, One-step ethylene production from a four-component gas mixture by a single physisorbent, Nat. Commun. 12 (2021) 6507.

[39] Y. Wang, M. Fu, S. Zhou, H. Liu, X. Wang, W. Fan, Z. Liu, Z. Wang, D. Li, H. Hao, X. Lu, S. Hu, D. Sun, Guest-molecule-induced self-adaptive pore engineering facilitates purification of ethylene from ternary mixture, Chem 8 (2022) 3263–3274.

[40] H.-T. Wang, Q. Chen, X. Zhang, M.-M. Xu, R.-B. Lin, H. Huang, L.-H. Xie, J.-R. Li, Two isostructural metal-organic frameworks with unique nickel clusters for $C_2H_2/C_2H_6/C_2H_4$ mixture separation, J. Mater. Chem. A 10 (2022) 12497-12502.

[41] S. Laha, N. Dwarkanath, A. Sharma, D. Rambabu, S. Balasubramanian, T. K. Maji, Tailoring a robust Al-MOF for trapping C_2H_6 and C_2H_2 towards efficient C_2H_4 purification from quaternary

mixtures, Chem. Sci. 13 (2022) 7172-7180.

[42] P. Liu, Y. Wang, Y. Chen, J. Yang, X. Wang, L. Li, J. Li, Construction of saturated coordination titanium-based metal-organic framework for one-step $C_2H_2/C_2H_6/C_2H_4$ separation, Sep. Purif. Technol. 276 (2021) 119284.

[43] E. Wu, X.-W. Gu, D. Liu, X. Zhang, H. Wu, W. Zhou, G. Qian, B. Li, Incorporation of multiple supramolecular binding sites into a robust MOF for benchmark one-step ethylene purification, Nat. Commun. 14 (2023) 6146.

[44] Y. Xiong, C.-X. Chen, T. Pham, Z.-W. Wei, K. Forrest, M. Pan, C.-Y. Su, Dynamic spacer installation of multifunctionalities into metal-organic frameworks for spontaneous one-step ethylene purification from a ternary C_2-hydrocarbons mixture, CCS Chem. 6 (2023) 241-254.